Journal of Petroleum Science and Engineering 131 (2015) 96–113

Contents lists available at ScienceDirect

Journal of Petroleum Science and Engineering

journal homepage: www.elsevier.com/locate/petrol

Modeling of capacitance flow behavior in EOS compositional simulation

Bo Zhang, Ryosuke Okuno *

School of Mining and Petroleum Engineering, University of Alberta, Edmonton, Alberta, Canada T6G 2W2

ARTICLE INFO

Article history:
Received 2 October 2014
Accepted 10 April 2015
Available online 22 April 2015

Keywords:
Gas injection
Fluid characterization
Equations of state
Bypassed oil recovery
Compositional flow simulation

ABSTRACT

Gas injection is a widely used method for enhanced oil recovery. Oil bypassing by gas occurs at different scales because of micro and macroscopic heterogeneities, gravity segregation, and front instability. Part of the bypassed oil can be recovered by crossflow between the bypassed and flowing regions. This characteristic of reservoir flow is referred to as capacitance flow behavior in the literature. Modeling of such flow behavior at the sub-grid scale is challenging in the conventional flow simulation since fluids are perfectly mixed and in equilibrium within individual grid blocks under the local equilibrium assumption.

This research investigates capacitance flow behavior in compositional reservoir simulation. An efficient two-step method is presented to model bypassed oil recovery in multiphase compositional flow simulation of gas floods. The oil bypassing is first quantified by use of the dual-porosity flow with two dimensionless groups; bypassed fraction and throughput ratio. To represent bypassed oil recovery in single-porosity flow, a new flow-based fluid characterization is applied to part of the heavy fractions of the fluid model used. Properties for pseudo components can be determined based on the throughput ratio estimated in the dual-porosity flow. Case studies for various reservoir/fluid properties show that single-porosity flow with the new method reasonably represents bypassed oil recovery observed in core floods and fine-scale heterogeneous simulations.

1. Introduction

Gas injection is a widely used method for enhanced oil recovery. The interplay of fluid flow with phase behavior can yield multicontact miscibility between reservoir oil and injection gas (Johns, 1992; Dindoruk, 1992; Orr, 2007). Therefore, design of gas injection processes often requires compositional simulation that can accurately model properties of equilibrium phases by use of a cubic equation of state (EOS) (Coats, 1980; Watts, 1986; Collins et al., 1992). Compositional simulation attempts to consider various complexities that exist in actual reservoir processes by increasing the generalization level of the conservation equations. (Chang et al., 1990; Cao, 2002). Fundamental assumptions always made include the local equilibrium assumption, where fluids are perfectly mixed and in equilibrium within individual continua (i.e., grid blocks) (Lake, 1989).

The continuum assumption is made to calculate large-scale fluid flow in porous media with a finite-difference scheme, in which grid blocks are greater than a representative elementary volume (REV) (Lake, 1989; Hill, 1963). The local discontinuities of an actual porous medium are not taken into account under the continuum assumption. The grid-block scales in a practical finite-difference reservoir simulation are much greater than the REV (Salehi et al., 2013). Fluid properties in a grid block at each time step are then calculated with the local equilibrium assumption, where the thermodynamic equilibrium is calculated for a given set of overall composition, pressure, and temperature.

Oil bypassing by gas occurs at different scales because of micro and macroscopic heterogeneities, gravity segregation, and front instability. It has been observed in various types of experiments and field applications of gas injection. Flow-visualization experiments (Stalkup, 1970; Chatzis et al., 1983; Campbell and Orr, 1985; Bahralolom et al., 1988; Stern, 1991) showed that microscopic oil bypassing was related to pore structures with bimodal or wide pore-size distributions. Shielding of oil by water films in pores can also hinder the contact between the bypassed oil and injection gas in the region with high water saturations (Shelton and Schneider, 1975; Spence et al., 1980; Wylie and Mohanty, 1997; Wylie and Mohanty, 1999). These results clearly indicate that oil bypassing is present even at the microscopic scale smaller than a REV.

At macroscopic scales greater than a REV, gas channeling creates slow-flow or stagnant regions in heterogeneous reservoirs (Cinar et al., 2006; Al-Wahaibi et al., 2007). Thin shales with a thickness of only a

* Correspondence to: 3-114 Markin/CNRL, Natural Resources Engineering Facility, University of Alberta, Edmonton, Alberta, Canada T6G 2W2. Tel.: +1 780 492 6121.
E-mail address: rokuno@ualberta.ca (R. Okuno).

http://dx.doi.org/10.1016/j.petrol.2015.04.014
0920-4105/

Nomenclature

Roman Symbols

A	Area
A_m	Dimensionless attraction parameter for mixtures
a_i	Attraction parameter for component i in a cubic equation of state
B	Bypassed fraction
b_i	Covolume parameter for component i in a cubic equation of state
c_{Dh}	Dimensionless volume-shift parameter of introduced pseudo heavy components
c_{hi}	Volume-shift parameter of component hi
e	Coefficient defined for permeability correlation
f	Exponent defined for permeability correlation
K	Permeability
$\vec{n}$	Outward unit normal vector
n_c	Number of components
n_p	Number of phases
P_{C_T}	Critical pressure
$\vec{q}_{ij}$	Molar flux vector of component i in phase j from the flowing fraction to the bypassed fraction
R_T	Throughput ratio
S	Surface area
S_C	Surface area of coarse-scale grid block
S_j	Saturation of phase j
t	Time
t_D	Dimensionless time
T_C	Critical temperature
$\vec{U}_j$	Flow velocity of phase j
V	Volume
V_C	Volume of coarse-scale grid block
x_{ij}	Mole fraction of component i in phase j
x_D	Dimensionless distance
z_i	Overall mole fraction of component i

Abbreviations

DPF	Dual-porosity flow
EOS	Equation of state
MMP	Minimum miscibility pressure
PC	Pseudo component
PR	Peng-Robinson
PVI	Pore-volume injected
SPF	Single-porosity flow

Greek symbols

φ	Porosity
ρ_j	Molar density of phase j
γ_a	Attraction-parameter index
γ_h	Molar-ratio index

Subscripts/superscripts

B	Bypassed fraction
D	Dimensionless
F	Flowing fraction
hi	Introduced heavier oil component i
i	Component i
j	Phase j
m	Mixture
oi	Original oil component i
T	Transverse direction

few inches can cause marked oil bypassing by gas (McGuire et al., 1995). Front instability can also lead to oil bypassing, if the mobility ratio between the injection gas and reservoir oil is large (Gardner and Ypma, 1984; Brock and Orr, 1991).

Part of bypassed oil can be recovered by the transverse mass flux between the bypassed and flowing regions as reported by a number of researchers (Pande, 1992; Pande and Orr, 1994a, 1994b; Burger et al., 1994, 1996; Burger and Mohanty, 1997; Zhou et al., 1997; Cinar et al., 2006; Al-Wahaibi et al., 2007). The transverse flux between the two regions can occur because of diffusion, dispersion, viscous forces, and capillarity [Pande, 1992; Pande and Orr, 1994a, 1994b]. Gradual migration of oil from the bypassed region to the flowing region can cause the resulting composition profile to deviate from the one without the transverse mass flux (Brock and Orr, 1991; Pande and Orr, 1994a; 1994b; Zhou et al., 1997). High residual oil saturations were observed in dominant flow paths due to the interaction of phase behavior with oil bypassing (Gardner and Ypma, 1984; Campbell and Orr, 1985; Bahralolom et al., 1988; Mohanty and Johnson, 1993). These results indicate the importance of considering the effects of oil bypassing on oil recovery.

The degree of miscibility between oil and gas also affects the level of bypassing in gas floods (Mohanty and Johnson, 1993; Burger and Mohanty, 1997). Experimental results (Burger et al., 1994) showed that the bypassed-oil fraction was smaller for less miscible processes. It was stated that the optimum gas enrichment can be below the minimum miscibility enrichment for a secondary gas flood with a high-viscosity ratio, where the sweep and local displacement efficiencies take a balance. In the mechanistic investigation of bypassed-oil recovery in CO_2 injection (Khosravi et al., 2014), a maximum recovery was achieved at sub-miscible conditions, where the oil swelling and vaporization enhanced the recovery of bypassed oil significantly. Also, it is not always economical or technically feasible to inject a gas that is miscible with oil (Bardon et al., 1994; Al-Wahaibi et al., 2007; Ren et al., 2011). In this research, the focus is on gas floods at sub-miscible (or immiscible) conditions.

The key characteristic of reservoir flow with oil bypassing is that the oil held in the bypassed (slow-flow or stagnant) region is gradually migrated to the flowing region through the transverse mass flux between the bypassed and flowing regions. This flow behavior has been referred to as capacitance. The capacitance flow behavior observed in core floods has been studied by use of mathematical models since late 1950s. The capacitance flow was observed as earlier breakthrough of the displacing component and longer tailing of the effluent-concentration history for the displaced component (Coats and Smith, 1964; Barker, 1977). The convection-dispersion model (Aronofsky and Heller, 1957) was confirmed to be incapable of reproducing the asymmetrical effluent-concentration histories of core-flood experiments (Coats and Smith, 1964; Barker, 1977; Zhang, 2014).

Deans (1963) proposed a capacitance model for single-phase flow, in which the pore volume was divided into the flowing and bypassed fractions. The longitudinal convection occurred only in the flowing fraction. Effective mass transfer coefficients were used to model the local transverse mass flux between the two regions. Coats and Smith (1964) included the longitudinal dispersion for the flow fraction on the basis of the capacitance model of Deans

(1963). The dispersion–capacitance model was successful in matching the asymmetrical effluent-concentration histories of core-flood experiments. The key dimensionless groups in the dispersion–capacitance model are flowing fraction, Péclet number, and Damkhöler number. Damkhöler number is the dimensionless mass-transfer rate expressed as a ratio of characteristic times for transverse mass transfer and longitudinal convection (Dai and Orr, 1987). The dispersion–capacitance model was extended and applied to study various non-uniform flow problems (Salter and Mohanty, 1982; Dai and Orr, 1987; Smith and Jikich, 1994; Nguyen et al., 2009). However, it has not yet been applied in compositional reservoir simulation.

Reservoir simulation can consider explicitly the level of heterogeneity at the scale of grid blocks and greater. However, modeling of capacitance flow behavior caused by sub-grid physics is challenging in reservoir simulation. The oil bypassing caused by front instability in gas floods was modeled by empirical viscous-fingering models (Koval, 1963; Todd and Longstaff, 1972; Young, 1990; Fayers et al., 1992; Blunt and Christie, 1994; Barker and Evans, 1995). However, such a model was not entirely satisfactory without the diffusion/dispersion term in large amplitude heterogeneities with a short correlation length (Fayers et al., 1992).

Modeling of capacitance flow behavior in compositional reservoir simulation is important since compositional simulation with a detailed geological model is computational expensive (Salehi et al., 2013; Iranshahr et al., 2014). Various modeling methods relevant to this technical issue can be categorized into four types, although the demarcation cannot be entirely clear. A first type is the S_{orm} method, which is available in commercial simulators to model oil-bypassing (Hiraiwa and Suzuki, 2007; Lizuka et al., 2012). It excludes the immobile oil from flash calculations so that this part of oil cannot be recovered. The main disadvantage of this method is that no mass flux is allowed between the bypassed and flowing fractions. The S_{orm} method is equivalent to assigning zero to the Damköler number in the dispersion–capacitance model. Thus, although oil bypassing can be considered, the bypassed oil is unrecoverable.

A second type is the method of Barker and Fayers (1994), which has been implemented in commercial simulators. This method uses the transport coefficients (alpha factors) to adjust the components' flux in compositional reservoir simulation. Barker et al. (2005) mentioned that this is a purely numerical concept; it is physically impossible to control the mass flux of certain components in a phase in given region of a reservoir. The alpha-factor method has been used to retain a desired amount of residual oil in history matching for predominantly single-phase flow (Ballin et al., 2002). Pseudo relative permeabilities are required at sub-miscible conditions. The presence of more phases yields more non-linearity and severer non-uniqueness of the history matching process with the alpha factors (Barker and Fayers, 1994; Christie and Clifford, 1998; Barker et al., 2005; Bourgeois et al., 2011, 2012). Christie and Clifford (1998) combined the alpha-factor method with streamline techniques, and re-calculated the boundary conditions for certain grid blocks to deal with the potential error in multidimensional cases.

Modeling of capacitance at the sub-grid scale is difficult because the mass conservation equations used in compositional reservoir flow simulation do not consider the bypassed fraction and the mass transfer between the bypassed and flowing fractions. A third type of methods is to introduce one more continuum to represent a bypassed fraction of the reservoir volume. The mass flux between the flowing and bypassed fractions can represent the non-equilibrium behavior at the sub-grid scale. Fayers et al. (1989) proposed the dual-zone-mixing procedure, in which a gridblock is split into the contacted and bypassed zone with separate flash calculations performed. Nghiem and Sammon (1997) developed a non-equilibrium EOS compositional simulator, and introduced a transfer term to represent the diffusion process at the oil–gas interface. Compositional flow using the dual-porosity model is likely the most straightforward representation of oil bypassing and recovery of the bypassed oil (i.e., capacitance) in gas injection (Coats et al., 2007). The dual-porosity method was used to track the changes in the compositions of the trapped and mobile fluids in WAG injection (Brown et al., 2013). However, the dual-porosity model may be too time-consuming to be used for field-scale applications (Coats et al., 2007). Apart from the computational efficiency, a single-porosity model may be preferred in terms of the computational robustness; in Peng et al. (2009), for example, the dual-porosity model had convergence issues in simulating strongly heterogeneous reservoirs.

A fourth type of methods is to adjust thermodynamic properties of components to match fine-scale fluxes in a coarse-scale simulation. Camy and Emanuel (1977) applied pseudo *K*-values obtained from a 1-D representative model for gas flooding. It also required pseudo gas-oil relative permeability and components' correction factors to reduce the deviation of coarse-scale results from fine-scale results. Recently, a novel upscaling algorithm was developed on the basis of non-equilibrium thermodynamics

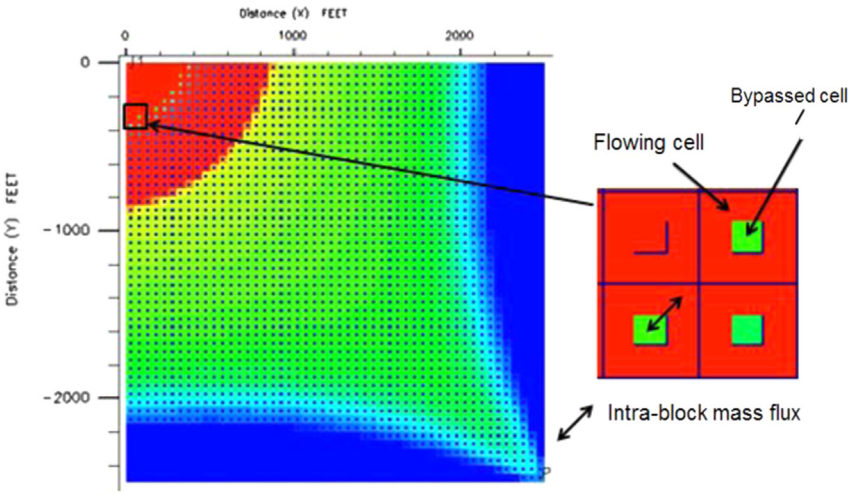

Fig. 1. Schematic of 2-D dual-porosity flow (DPF). Each grid block consists of the flowing and bypassed fractions. The bypassed fraction does not contribute to the longitudinal convection. The intra-block mass flux allows for the gradual migration of the bypassed oil to the flowing fraction.

(Iranshahr et al., 2014). Phase-equilibrium constraints were adjusted to correct the difference in phase behavior between the coarse- and fine-scale models. The thermodynamically-consistent alpha-factor method was then developed using their non-equilibrium approach to upscale near-miscible gas injection processes (Salehi et al., 2013).

This paper presents a two-step method, which combines the third and fourth types of methods, to efficiently model the sub-grid-scale capacitance by use of the conventional compositional simulation. The first step is to quantify capacitance flow behavior in a reservoir by use of the dual-porosity flow (DPF) model with two dimensionless groups. The second step is to correct the fluid model used in the simulation for the quantified capacitance flow behavior using a flow-based fluid characterization method. Case studies are presented to show that SPF with the two-step method can quantitatively reproduce capacitance flow behavior present in core floods and fine-scale simulations. The main novelty of the research lies in the way of representing capacitance flow behavior by controlling components' in-situ propagation through EOS-related parameters.

2. Quantification of capacitance flow behavior by use of dual-porosity flow

This section describes dual-porosity flow (DPF) and its application for capturing capacitance flow behavior in heterogeneous fine-scale simulations. Capacitance flow behavior occurs when the oil held in the bypassed (slow-flow or stagnant) region is gradually migrated to the flowing (fast-flow) region (Coats and Smith, 1964; Barker, 1977). Modeling of capacitance flow behavior at the sub-grid scale is difficult in single-porosity flow (SPF) simulation due to the local equilibrium assumption within individual grid blocks.

One way to capture such flow behavior is to use DPF simulation (Coats et al., 2007), where the primary- and secondary-pore systems represent the flowing and bypassed fractions, respectively. Oil in the flowing fraction is directly displaced by the injectant. The bypassed fraction has no contribution to the longitudinal convection. The two fractions have intra-block mass flux in the transverse direction within individual grid blocks. The DPF model is capable of representing the flow characteristics of the dispersion–capacitance model, since the bypassed oil held up in the secondary-pore volume (the bypassed fraction) is gradually migrated to the primary-pore volume (the flowing fraction) through intra-block mass flux. Fig. 1 schematically shows a 2-D DPF model.

2.1. Material balance equations

A DPF model for capturing capacitance flow behavior can be explained by comparing material balances applied to SPF and DPF. The molar balance for component i for a grid block with volume V and surface area S in SPF is

$$\frac{d}{dt}\int_V \left(\varphi \sum_{j=1}^{n_p} x_{ij}\rho_j S_j\right) dV + \int_S \sum_{j=1}^{n_p} \left[\vec{n}\cdot\left(x_{ij}\rho_j \vec{U}_j\right)\right] dA = 0 \quad (1)$$

where $i=1, 2,\ldots, n_c$, and $j=1, 2, \ldots, n_p$. n_c and n_p are the numbers of components and phases, respectively. The first term is the accumulation term, and the second term is the convective flux term. The physical diffusion/dispersion term is neglected in the equation. Symbols are defined in the nomenclature section.

Suppose that grid blocks are grouped into a coarse-scale grid block with volume V_C and surface area S_C (i.e., $V_C > V$). This grid block consists of the flowing and bypassed fractions; that is, a dual-porosity model is applied. The volume and surface area are split into two fractions; V_{CF} and S_{CF} for the flowing fraction and V_{CB} and S_{CB} for the bypassed fraction. Then, the molar balance for component i for this coarse-scale grid block is

$$\frac{d}{dt}\left[\int_{V_{CF}} \left(\varphi \sum_{j=1}^{n_p} x_{ij}\rho_j S_j\right) dV + \int_{V_{CB}} \left(\varphi \sum_{j=1}^{n_p} x_{ij}\rho_j S_j\right) dV\right] + \int_{S_{CF}} \sum_{j=1}^{n_p} \left[\vec{n}\cdot\left(x_{ij}\rho_j \vec{U}_j\right)\right] dA = 0. \quad (2)$$

The flux term is only for the flowing fraction since the bypassed fraction does not contribute to the inter-block flux.

The molar balance for component i for the bypassed fraction of the coarse-scale grid block (V_{CB}) is

$$\frac{d}{dt}\int_{V_{CB}} \left(\varphi \sum_{j=1}^{n_p} x_{ij}\rho_j S_j\right) dV - \int_{S_{CB}} \sum_{j=1}^{n_p} \left(\vec{n}\cdot\vec{q}_{ij}^{\,T}\right) dA = 0, \quad (3)$$

where $\vec{q}_{ij}^{\,T}$ in the second term is the molar flux vector of component i in phase j from the flowing fraction to the bypassed fraction within this coarse-scale grid block. The positive direction

Table 2
Properties for three-component n-alkane mixtures.

	Oil (mole fraction)	Gas (mole fraction)	Molecular weight (g/mol)	T_C (°F)	P_C (psia)	ω	Critical volume (ft^3/lb-mol)
C_1	0.2	0.0	16.043	−116.590	667.20	0.0080	1.59
C_2	0.0	1.0	30.070	90.050	708.35	0.0980	2.37
C_{10}	0.8	0.0	142.285	644.620	321.78	0.5032	9.66

Table 1
Reservoir properties for 1-D dual porosity simulation.

Dimensions (F*/B*)	$2 \times 900 \times 50$ ft^3/$2 \times 100 \times 50$ ft^3
Number of gird blocks	$500 \times 2 \times 1$
Porosity	0.3
Permeability (F*/B*)	2000 md (X,Z), 2000 md(Y)/0.0 md(X,Z), 0.2 md (Y)
Reservoir pressure	1015.27 psia
Reservoir temperature	158°F
Injection pressure	1025.27 psia
Production pressure	1015.27 psia
Relative permeability model	Corey
Residual saturation (Oil/Gas)	0.24/0.0
Endpoint relative permeability (Oil/Gas)	1.0/0.6
Exponent (Oil/Gas)	2.1/1.8
Initial saturation (Oil/Gas)	1.0/0.0
Molecular diffusion coefficents in oil phase (C_1/C_2/C_{10})	0.002575/0.001465/0.000625 ft^3/day
Molecular diffusion coefficents in gas phase (C_1/C_2/C_{10})	25.75/14.65/6.25 ft^3/day
*F: Flowing grid block; *B: Bypassed grid block.	

for the intra-block flux was defined merely for a notational convenience. Using Eqs. (2) and (3), the molar balance of component i for the flowing fraction of the coarse-scale grid block (V_{CF}) is written as

$$\frac{d}{dt}\int_{V_{CF}}\left(\varphi\sum_{j=1}^{n_p}x_{ij}\rho_j S_j\right)dV+\int_{S_{CF}}\sum_{j=1}^{n_p}\left[\vec{n}\cdot\left(x_{ij}\rho_j\vec{U}_j\right)\right]dA+\int_{S_{CB}}\sum_{j=1}^{n_p}\left(\vec{n}\cdot\vec{q}^{\,T}_{ij}\right)dA=0. \tag{4}$$

The DPF model given in Eq. (4) will be able to reproduce the capacitance flow behavior that is present in the fine-scale model given in Eq. (1), if Eq. (4) matches the following balance equation for the group of fine-scale grid blocks:

$$\frac{d}{dt}\int_{V_C}\left(\varphi\sum_{j=1}^{n_p}x_{ij}\rho_j S_j\right)dV+\int_{S_C}\sum_{j=1}^{n_p}\left[\vec{n}\cdot\left(x_{ij}\rho_j\vec{U}_j\right)\right]dA=0. \tag{5}$$

The net molar fluxes out of volume V_C in the DP and SP models (i.e., the second terms of Eqs. (4) and (5)) become identical if

$$\frac{d}{dt}\int_{V_C}\left(\varphi\sum_{j=1}^{n_p}x_{ij}\rho_j S_j\right)dV=\frac{d}{dt}\int_{V_{CF}}\left(\varphi\sum_{j=1}^{n_p}x_{ij}\rho_j S_j\right)dV+\int_{S_{CB}}\sum_{j=1}^{n_p}\left(\vec{n}\cdot\vec{q}^{\,T}_{ij}\right)dA. \tag{6}$$

Eq. (6) indicates two important parameters for reproducing the coarse-scale flow behavior in the fine-scale SPF (i.e., Eq. (5)) by use of the coarse-scale DPF (i.e., Eq. 4). One is the flowing fraction to define V_{CF} ($=V_C-V_{CB}$) in the first term of the right-hand side of Eq. (6). The other is the intra-block molar flow rate, the second term of the right-hand side of Eq. (6).

One could attempt to satisfy Eq. (6) for each of the coarse-scale grid blocks if the bypassed fractions and intra-block molar flow rates were known for the grid blocks. This is similar to the capacitance-dispersion model, where Damkhöler number can control the intra-block mass-transfer rate locally. However, such information is usually unavailable. In this research, therefore, capacitance flow behavior is characterized at the scale of flow of interest; i.e., the core scale in core floods and the well-pattern scale in reservoir simulations. Then, Eq. (6) is applied to the entire volume at the flow scale, yielding two dimensionless parameters associated with capacitance flow behavior, which are bypassed fraction (B) and throughput ratio (R_T) as defined below.

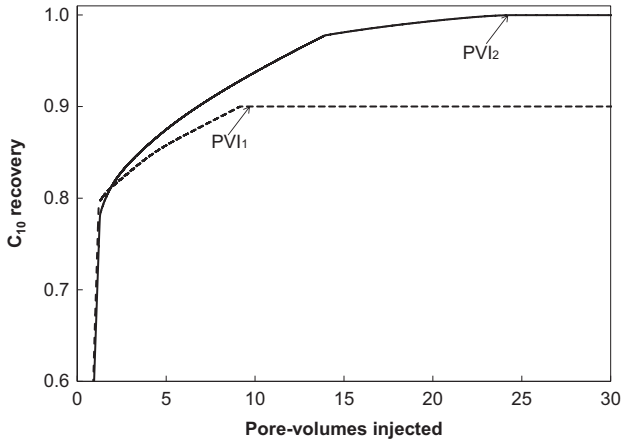

Fig. 2. C_{10} recovery predictions for 1-D DPF with/without the intra-block mass flux. PVI_1 and PVI_2 represent the pore-volumes injected required for the ultimate recovery without/with the intra-block mass flux in DPF, respectively. Tables 1 and 2 give the simulation conditions and fluid properties, respectively.

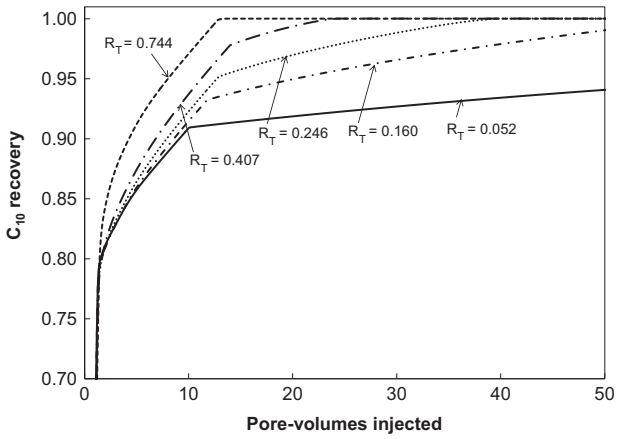

Fig. 3. C_{10} recovery predictions for 1-D DPF with different values of the throughput ratio (R_T) from 0.052 to 0.744. Oil recoveries with different levels of capacitance are well characterized by R_T for a given bypassed fraction. Tables 1 and 2 give the simulation conditions and fluid properties, respectively. For simulations with different R_T values, the intra-block mass flux was adjusted by multiplying the diffusion coefficients by different constants as described in Zhang (2014).

2.2. Dimensionless groups

Bypassed fraction (B) is V_B/V, where V_B is the bypassed volume within volume V. The same definition was used in the literature (Stern, 1991; Lange, 1998). Lange (1998) presented a correlation for estimating the bypassed fraction based on gas solubility in oil, gas density, and average molecular weight of oil. Note that a single value of B is determined to a given flow in this research since flow characterization is made globally at the flow scale.

Throughput ratio (R_T) is defined as PVI_1/PVI_2, where PVI_1 and PVI_2 are the pore-volumes injected (i.e., throughputs measured in pore volumes) required for ultimate oil recovery without and with intra-block flux in the DPF, respectively. R_T is zero for no intra-block mass flux, which corresponds to SPF with the S_{orm} method. R_T becomes unity as the intra-block mass flux approaches infinity. Thus, SPF without the S_{orm} method has a limiting R_T of unity since equilibrium is instantaneously achieved within individual grid blocks with the local equilibrium assumption.

R_T represents the ratio of characteristic time for intra-block mass flux and mass flux in the longitudinal direction in DPF. This is a gross form of Damkhöler number in the dispersion–capacitance model; i.e., R_T is measured for the entire flow system of interest (e.g., a core, and a reservoir volume at a drive-pattern scale), and Damkhöler number is defined locally. Unlike the traditional SPF models with and without the S_{orm} method, the DPF model can represent capacitance flow behavior with any R_T value between 0.0 and 1.0 for a given bypassed fraction.

For further description of R_T, simple 1-D simulations are used here. Table 1 shows the reservoir properties used for the 1-D DPF simulations. For the 1-D SPF simulations, the bypassed fraction is simply set to zero while keeping the reservoir dimensions. Phase behavior of the ternary system given in Table 2 is calculated using the Peng-Robinson (PR) EOS (Peng and Robinson, 1976) with the van der Waals mixing rules. C_2 is injected to displace the reservoir oil consisting of 20% C_1 and 80% C_{10}. The reservoir temperature and pressure are 158°F and 1015.27 psia, respectively. The pressure is fixed at 1025.27 psia for the injector and at 1015.27 psia for the producer to control the effects of pressure on phase behavior. The minimum miscibility pressure (MMP) for this displacement is calculated to be 1174.27 psia using the tie-line approach within the PVTsim software (PVTsim, 2011). Viscosity calculations are based on the Lohrenz–Bray–Clark method (Lohrenz et al., 1964). The Wilke–Chang correlation (Wilke and Chang, 1955) is used to

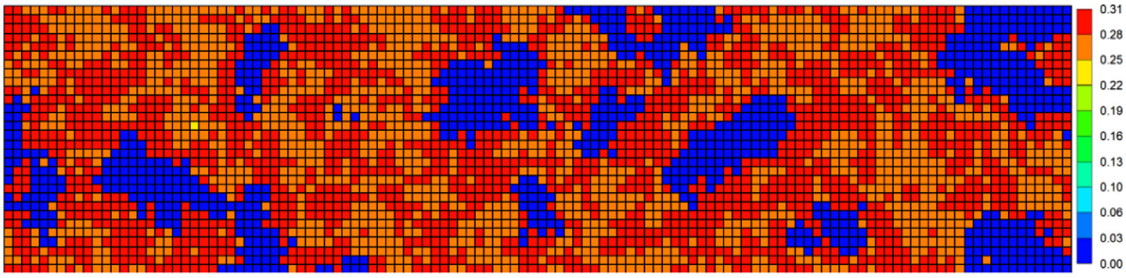

Fig. 4. Porosity distribution for the areal 2-D reservoir. The reservoir consists of 20% shale and 80% sandstone with a correlation length of 10 ft. Gas is injected along the left edge of the reservoir model.

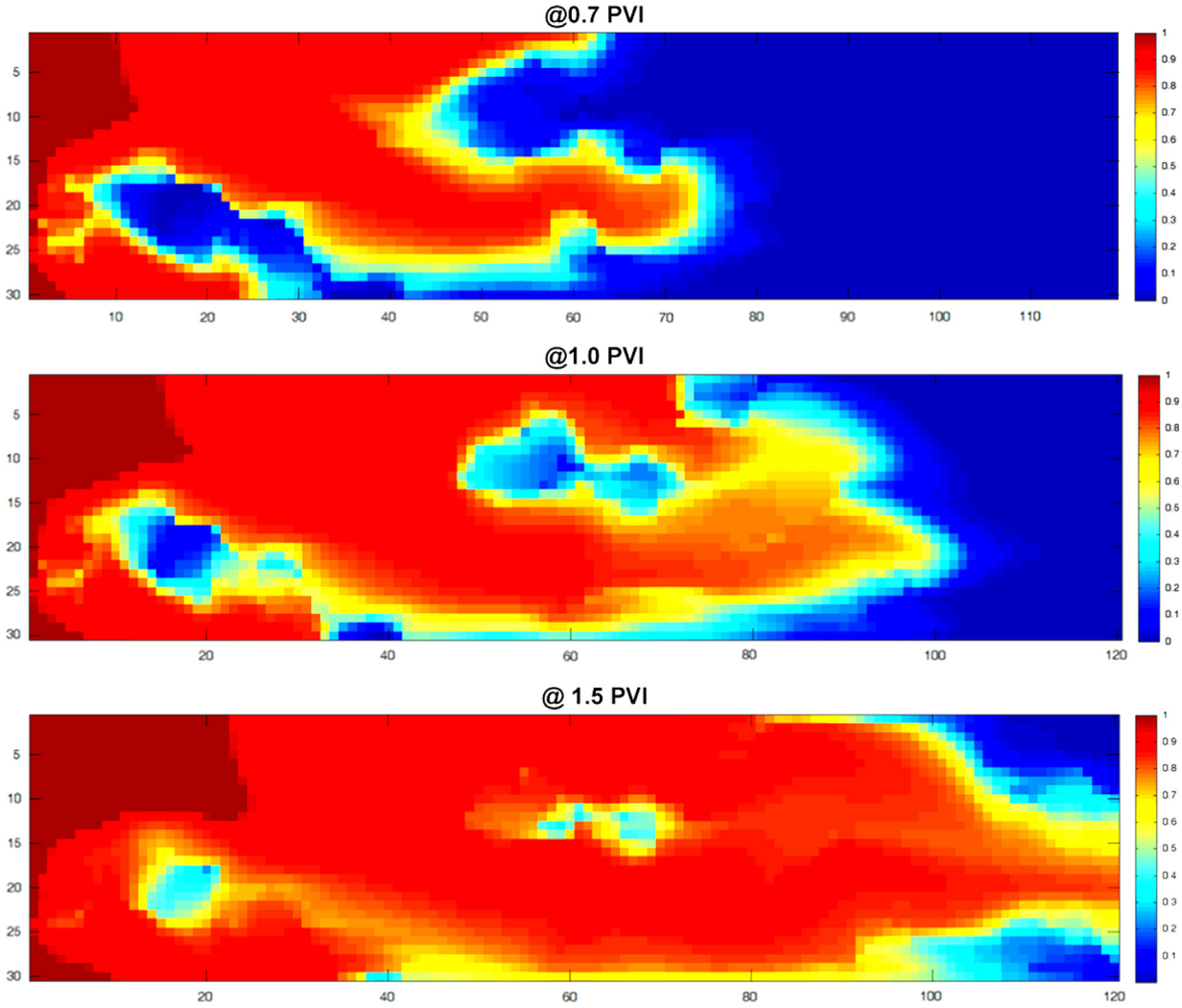

Fig. 5. C_2 concentration distributions in the fine-scale simulation case 1 at different PVIs. The fluid model used is presented in Table 2. Oil bypassing due to channeling is observed at 0.7 PVI, and the bypassed oil is gradually recovered at later times.

estimate the diffusion coefficients listed in Table 1. All flow simulations in this research are performed using Eclipse 300 of Schlumberger (Eclipse 300, 2010) with the fully implicit scheme with the single-point upstream weighting for relative mobilities.

Fig. 2 shows C_{10} recoveries in the 1-D DP model with and without intra-block mass flux. In this example, PVI_1 and PVI_2 are 9.93 and 24.34, respectively. R_T is then calculated to be 0.408. Fig. 3 presents C_{10} recoveries with different R_T values. Oil recoveries with different degrees of capacitance are well characterized using R_T. These different R_T values are generated by multiplying the intra-block diffusion coefficients (see Table 2) by factor C (e.g., C is zero for $R_T=0$). This method of controlling R_T is also used in the subsequent sections.

In this research, the longitudinal dispersion is controlled by the number of grid blocks using a uniform time step and grid block size. The longitudinal Péclet number is approximated to be $2/(\Delta x_D+\Delta t_D)$

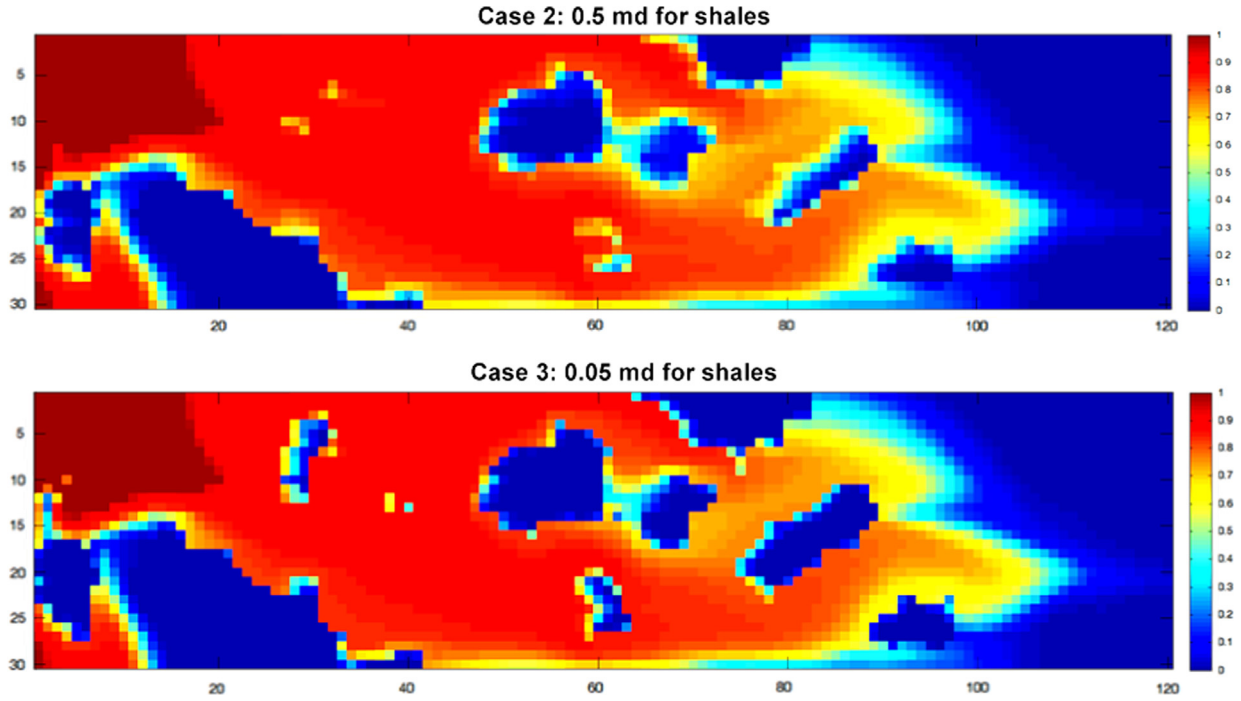

Fig. 6. C_2 concentration distributions in the fine-scale simulation cases 2 and 3 at 1.0 PVI. The fluid model used is presented in Table 2. The oil recovery from the bypassed (or slow-flow) regions is dependent on the shale permeability that affects the mass flux between the slow-flow and fast-flow regions. This can be confirmed by comparing with case 1 (5 md for shales) given in Fig. 5.

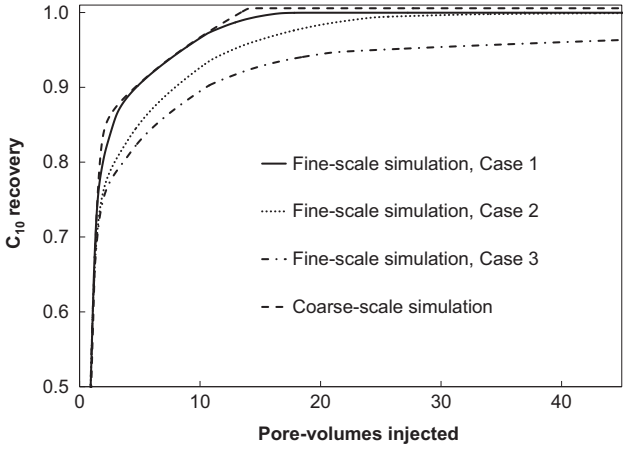

Fig. 7. Oil recovery predictions for the fine-scale simulation cases 1, 2, and 3 compared with the coarse-scale simulation. The fluid model used is presented in Table 2. The permeability of the shale region greatly affects the oil recovery from the bypassed (slow-flow) region. The coarse-scale simulation overestimates the oil recovery because it cannot consider the sub-grid scale capacitance flow behavior.

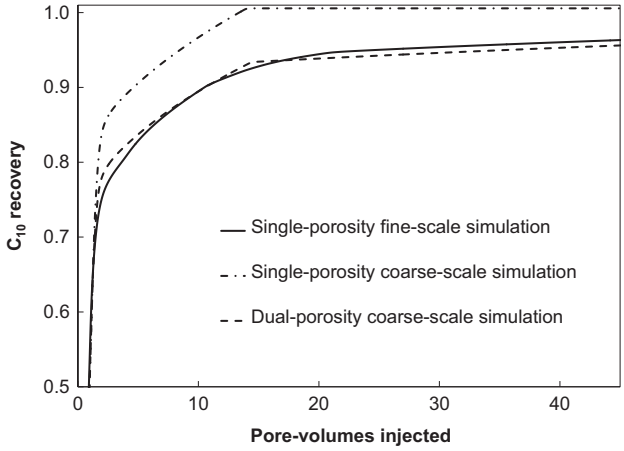

Fig. 8. Oil recovery predictions for the fine-scale simulation case 3 and the coarse-scale DPF and SPF simulations. The fluid model used is presented in Table 2. The DPF greatly improve the recovery prediction for the coarse-scale simulation because it accommodates the sub-grid scale capacitance flow behavior. The resulting throughput ratio and bypassed fraction are 0.14 and 0.08, respectively.

in the fully implicit simulations in this research, where Δx_D is the dimensionless grid-block size and Δt_D is the dimensionless time-step size measured in pore volumes (Lantz, 1971).

2.3. *Capacitance flow behavior in fine-scale simulation*

This subsection presents capacitance flow behavior observed in example fine-scale simulations. The DPF is then used to quantify the capacitance flow behavior.

The areal 2-D reservoir model consists of 120 grid blocks in the x direction and 30 grid blocks in the y direction. The dimensions of each grid block are $1.0 \times 1.0 \times 1.0$ ft^3. The porosity field has been generated by use of S-GeMS ver. 2.1 (S-GeMS V2.1), assuming a bimodal distribution consisting of 80% sandstone and 20% shale. The average porosity is 0.280 for sandstone and 0.019 for shale. The variance is 0.00012 for sandstone and 0.00002 for shale. The average porosity is 0.227, and the variance is 0.0118 for the 2-D reservoir model. The correlation length is 10.0 ft in the x and y directions. The porosity distribution used is shown in Fig. 4. The shales are shown in blue. Gas is injected along the left edge, and oil is produced along the right edge of the reservoir model.

Permeability distributions are calculated using the following widely-used correlation (Leung and Srinivasan, 2011; Leung and Srinivasan, 2012): $K = e\varphi^f$, where K is permeability in mD and f is 1.2 in this research. Different values are used for e as follows:

Case 1. e = 1200 mD for sandstone and shale
Case 2. e = 1200 mD for sandstone and 120 mD for shale

Case 3. e=1200 mD for sandstone and 12 mD for shale.

The three cases have the same porosity distribution and sandstone permeability.

The ternary fluid system given in Table 2 is used again. The reservoir temperature and pressure are 158°F and 1015.27 psia, respectively. C_2 is injected into the heterogeneous reservoir at partially miscible conditions. The oil and gas relative permeabilities are taken from Bardon et al. (1994).

Fig. 5 presents the C_2 concentration distributions for case 1 at different PVIs. The injected C_2 channels through the sandstone, and the oil near the shales is bypassed as shown at 0.7 PVI. The bypassed oil is gradually recovered because of the mass flux between the bypassed and flowing regions as shown at later PVIs. The recovery of bypassed oil is relatively fast in case 1 because of the relatively high permeability assigned to the shales (5 mD). Gas breakthrough occurs after 1.0 PVI because of the significant volume change on mixing in this fluid system.

C_2 concentration distributions for cases 2 and 3 at 1.0 PVI are presented in Fig. 6. Recovery of the bypassed oil depends substantially on the shale permeability used, because it controls the mass flux between the bypassed and flowing regions. For case 3 with the lowest shale permeability (0.05 mD), the bypassed oil was clearly observed even at 10.0 PVI in Figure 3.24 of Zhang (2014) Thus, modeling of bypassed oil recovery can greatly affect oil recovery predictions in gas injection simulation.

As well known in the literature, simplistic upscaling of a fine-scale reservoir model results in erroneous gas-flooding simulation results (Barker and Fayers, 1994). To confirm this, the fine-scale model was upscaled into a coarse-scale reservoir model with 12×3 grid blocks. The porosities of the coarse-scale model were calculated by the arithmetic mean in the corresponding regions of the fine-scale model. The permeability distribution for the coarse-scale model was then calculated by use of the equation $K=1200\varphi^{1.2}$ based on the upscaled porosity distribution.

Fig. 7 presents C_{10} recovery predictions from the fine-scale simulation cases 1, 2, and 3 along with the coarse-scale simulation with the upscaling presented previously. The simplistic upscaling gives a reasonable prediction only if the level of capacitance is insignificant (i.e., case 1). It substantially overestimates the oil recovery for cases 2 and 3.

As shown in Section 2.1, one way to improve the issues associated with the subgrid-scale capacitance is to use the DPF simulation. A DPF model with the coarse-scale reservoir model was fitted to the fine-scale simulation case 3 with the bypassed fraction of 0.08 and throughput ratio of 0.14. Fig. 8 shows that the resulting DPF model agrees well with the fine-scale simulation in terms of C_{10} recovery. The DPF parameters, such as B and R_T, are useful to quantify the capacitance flow behavior. The DPF parameters have been successfully applied to other cases, such as core floods, capillary dominant cases, and viscous dominant cases.

The uniform distribution of a bypassed fraction is sufficient to reproduce oil recovery as a function of throughput, as shown above. However, distribution of different bypassed fractions can be helpful in reproducing local concentration distributions by use of the coarse-scale DPF model. A detailed explanation of how to distribute different bypassed fractions can be found in Zhang (2014).

3. Flow-based fluid characterization

Section 2 presented that key characteristics of a given capacitance flow can be quantified by DPF with single average values of bypassed fraction (B) and R_T. However, it may be unacceptably time-consuming to run a DPF model for field-scale applications (Coats et al., 2007). Convergence issues may occur more often with highly heterogeneous reservoir models (Peng et al., 2009). Efficient modeling of capacitance flow behavior is a long-existing technical issue as pointed out by Burger et al. (1994).

As shown in Section 2, oil recovery with capacitance flow behavior takes more throughput than without it to achieve the same level of oil recovery. This was the fundamental idea used in the definition of R_T, which successfully quantifies the delayed oil recovery. Efficient modeling of sub-grid capacitance using a SPF model inevitably requires adjustment of components' propagation with respect to throughput in reservoir simulation. It is well-understood from the gas injection theory (Orr, 2007) that components' properties affect the dimensionless velocities (i.e., distances traveled at one pore volume injected) along the composition path for a partially miscible oil displacement by gas. Thus, one way to control components' propagation rates in reservoir simulation is to adjust their properties in the fluid model used.

The objective of flow-based fluid characterization in this research is to represent oil recovery that takes additional throughput in the presence of capacitance by adjusting components' properties in the fluid model used. The method attempts to minimize the deviation from the original fluid model of interest in terms of phase behavior predictions. Ideally, such deviation should be kept within the level of uncertainty inherent in characterization of reservoir oils.

3.1. Methodology

Properties are adjusted for some of the oil components; typically heavy pseudo components representing a plus fraction (e.g., C_{7+}). Each of adjusted components is split into two components; one with the original properties and the other with altered properties. This splitting is useful to retain the well-defined limiting properties in the case of no capacitance (i.e., $R_T=0$).

Adjustment of components' properties considers representation of DPF (Eqs. (2) or (4)) by use of SPF with the same coarse-scale grid blocks (with V_C and S_C), but with an altered fluid model. Here, it is assumed that capacitance flow behavior in the fine-scale model has been already reproduced by the coarse-scale DPF model (Eqs. (2) or (4)) by a certain set of bypassed fraction and R_T.

Oil component i is split into components "oi" and "hi" while retaining the total mass of the fluid of interest. Components oi and hi have the same molecular weight as the original oil component i. Component oi also has the same properties as the original oil

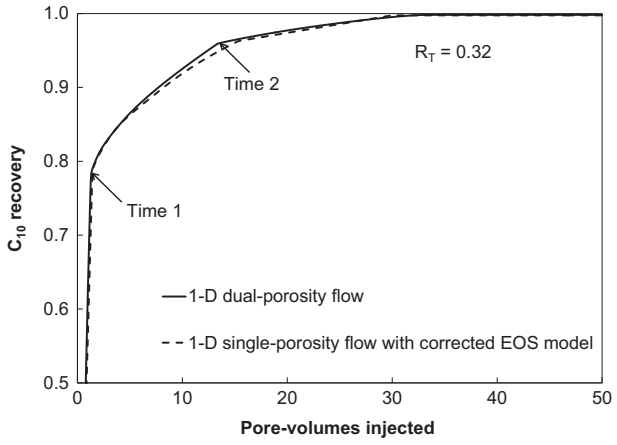

Fig. 9. C_{10} recovery predictions for the 1-D DPF and 1-D SPF with a corrected fluid model. Time 1 is the breakthrough time. Time 2 is the PVI when the evaporation wave in the flowing region reaches the outlet. After Time 2, the recovery comes from the bypassed oil. Tables 1 and 2 present the simulation conditions and fluid properties used, respectively.

component *i*. However, component hi has properties of a heavier component than component oi (and the original oil component *i*). The molar balance of component i, which now consists of oi and hi, for the coarse-scale grid block (with V_C and S_C) is

$$\frac{d}{dt}\int_{V_C}\left[\varphi\sum_{j=1}^{n_p}(x_{oij}+x_{hij})\rho_j S_j\right]dV+\int_{S_C}\sum_{j=1}^{n_p}\left\{\vec{n}\cdot\left[(x_{oij}+x_{hij})\rho_j\vec{U}_j\right]\right\}dA=0. \tag{7}$$

The molar fluxes out of volume V_C in Eqs. (4) and (7) become identical if

$$\frac{d}{dt}\int_{V_C}\left[\varphi\sum_{j=1}^{n_p}(x_{oij}+x_{hij})\rho_j S_j\right]dV=\frac{d}{dt}\int_{V_{CF}}\left(\varphi\sum_{j=1}^{n_p}x_{ij}\rho_j S_j\right)dV+\int_{S_{CB}}\sum_{j=1}^{n_p}\left(\vec{n}\cdot\vec{q}_{ij}^{\,T}\right)dA. \tag{8}$$

Using Eq. (3), it is easy to show that Eq. (8) is equivalent to

$$\frac{d}{dt}\int_{V_C}\left[\varphi\sum_{j=1}^{n_p}(x_{oij}+x_{hij})\rho_j S_j\right]dV=\frac{d}{dt}\left[\int_{V_{CF}}\left(\varphi\sum_{j=1}^{n_p}x_{ij}\rho_j S_j\right)dV+\int_{V_{CB}}\left(\varphi\sum_{j=1}^{n_p}x_{ij}\rho_j S_j\right)dV\right] \tag{9}$$

Properties of component hi are adjusted to approximately satisfy Eq. (9). The right-hand side of Eq. (9) shows that oil component i is held in V_{CB} that does not contribute to interblock fluxes. The left-hand side attempts to represent this capacitance by making the apparent properties of component *i* less volatile through component hi.

The thermodynamic model used in this research is the PR EOS with the van der Waals mixing rules. It is assumed that only one EOS fluid model is used for a given reservoir simulation. The attraction parameters of components hi's are adjusted through the attraction-parameter index γ_a defined as

$$\gamma_a=(a_{hi}-a_i)/(a_{hi}+a_i), \tag{10}$$

where a_{hi} and a_i are the attraction parameter of component hi and that of component i, respectively. The γ_a index is zero when $a_{hi}=a_i$, and tends to unity as a_{hi} becomes higher. Kumar and Okuno (2013) described the behavior of the PR attraction parameter for different carbon numbers and different levels of aromaticity. It monotonically increases with increasing carbon number for a fixed aromaticity level. A single value of γ_a is uniformly applied for all hi's in this research.

A more general approach is to adjust the attraction and covolume parameters of the PR EOS for components hi's. However, adjustment of the attraction parameters alone has been found to be sufficient to achieve the objective of the flow-based fluid characterization method in this paper. It is also desirable in reducing the deviation of phase behavior predictions from the original fluid model.

Once the properties of hi's are set through γ_a, the amounts of hi's relative to the original components are determined by adjusting the molar-ratio index γ_h defined as

$$\gamma_h=z_{hi}/(z_{oi}+z_{hi})=z_{hi}/z_i. \tag{11}$$

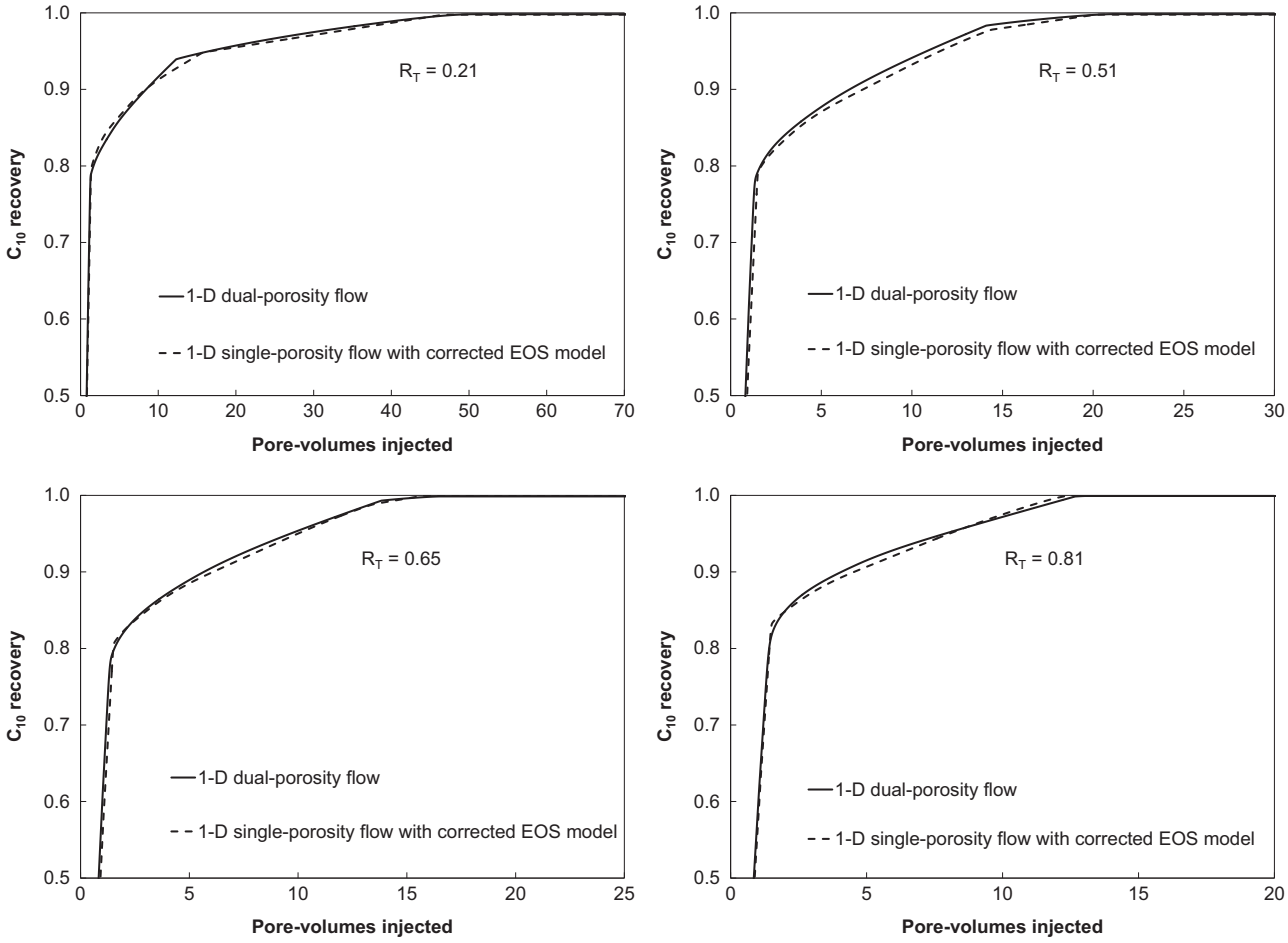

Fig. 10. C_{10} recovery predictions for 1-D DPF and 1-D SPF simulations with a corrected fluid model. The throughput ratios for the 1-D DPF simulations are 0.21, 0.51, 0.65, and 0.81. Tables 1 and 2 present the simulation conditions and fluid properties used, respectively. For simulations with different throughput ratios, the intra-block mass flux was adjusted by multiplying the diffusion coefficients by different constants as described in Zhang (2014).

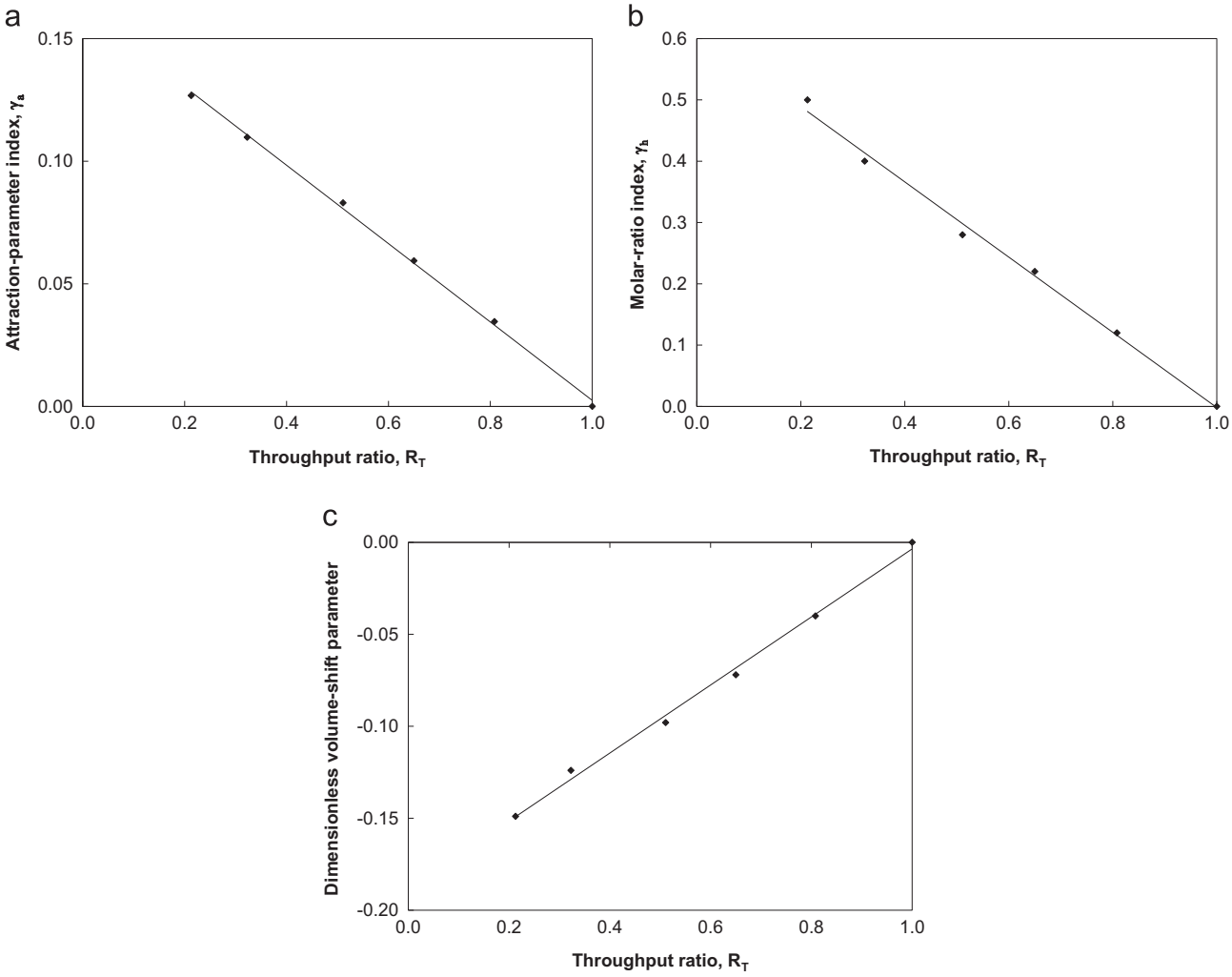

Fig. 11. Relationship between the throughput ratio (R_T) and three adjustment parameters; (a) Attraction-parameter index (γ_a) decreases with increasing R_T, (b) Molar-ratio index (γ_h) decreases with increasing R_T, and (c) Dimensionless volume-shift parameter (c_{Dh}) increases with R_T.

In Eq. (11), z_i is the mole fraction of component i, which is the summation of the mole fractions of components oi and hi, z_{oi} and z_{hi}. The γ_h index is zero when $z_{hi}=0$, and tends to unity as z_{hi} becomes higher. A single value of γ_h is uniformly applied for all adjusted components in this research.

Use of $\gamma_h > 0$ with $\gamma_a \neq 0$ gives the flexibility in compositional phase behavior predictions, which enables to control components' propagation in reservoir simulation. However, it also alters volumetric phase behavior (i.e., phase densities), and viscosity predictions through conventional viscosity models, such as the one by Lohrenz et al. (1964) as used in this research. It is possible to retain volumetric and viscosity predictions by use of volume shift. The dimensionless volume-shift parameter of component hi is

$$c_{Dh} = c_{hi}/b_i, \tag{12}$$

where c_{hi} is the volume-shift parameter of component hi, and b_i is the covolume parameter of component i. A single value of c_{Dh} is uniformly applied for all introduced components hi's in this research.

3.2. Algorithm

To explain the algorithm for the flow-based fluid characterization method, the example DPF with the ternary fluid system presented previously is used. Tables 1 and 2 give the simulation conditions and fluid properties used, respectively. The DPF with a throughput ratio of 0.32 is considered, for which Fig. 9 presents the oil recovery prediction. Time 1 is the PVI at the breakthrough, and Time 2 is when the evaporation wave reaches the outlet in the flowing fraction.

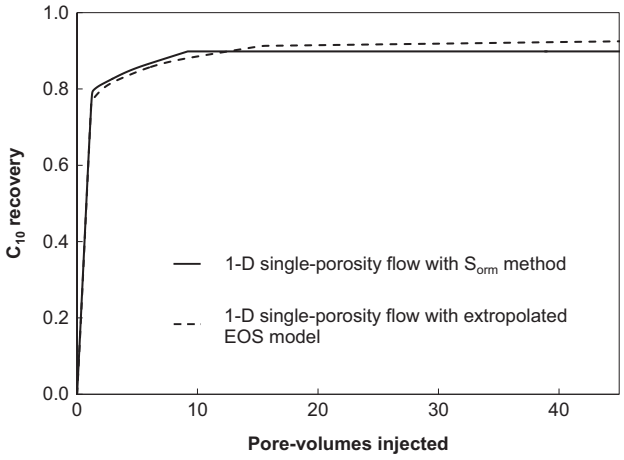

Fig. 12. C_{10} recovery prediction for the SPF simulation with the S_{orm} method is compared to that with a corrected fluid model extrapolated to R_T of zero. The linear extrapolation of the adjustment parameters to R_T of zero (see Fig. 11) gives reasonable representation of the limiting capacitance behavior, where the bypassed oil is unrecoverable as in the S_{orm} method. Tables 1 and 2 present the simulation conditions and fluid properties used, respectively.

The first step is to split C_{10} into C_{o10} and C_{h10}. A value of γ_a is estimated by matching the C_{10} recovery after Time 2. In this example, γ_a is 0.11. The dimensionless volume-shift parameter for C_{h10} is determined to retain the original oil density. The dimensionless volume-shift parameter for the injected gas component C_2 can be also adjusted to retain the oil recovery at the breakthrough time (Time 1 in Fig. 9). The last step is to determine γ_h to match the oil recovery between Time 1 and Time 2. For this selected case, γ_h is 0.4. Fig. 9 shows that the SPF with the corrected fluid model accurately matches the recovery prediction of the DPF model with a throughput ratio of 0.32.

A step-wise description of the algorithm for a general multi-component case is as follows:

Step 1. Split the pseudo components (representing the plus fraction) in the fluid model of interest into two fractions; one with the original properties and the other with altered properties. That is, pseudo component i is split into components "oi" and "hi." The mass of component i is retained; $z_i = z_{oi} + z_{hi}$, and molecular weights of oi and hi are the same as that of i.
Step 2. Adjust the γ_a index by matching the oil recovery prediction from DPF after Time 2, when the behavior of delayed oil recovery is easily captured.

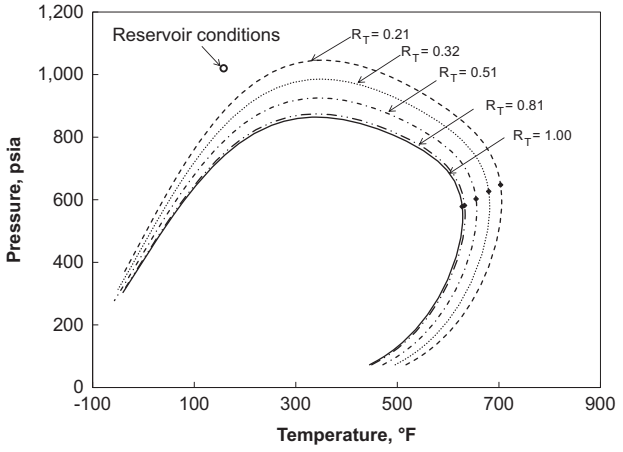

Fig. 13. Two-phase envelopes predicted for the oil (given in Table 2) with corrected fluid models with different throughput-ratio (R_T) values from 0.21 to 1.0. The deviation of the two-phase envelope increases with decreasing R_T.

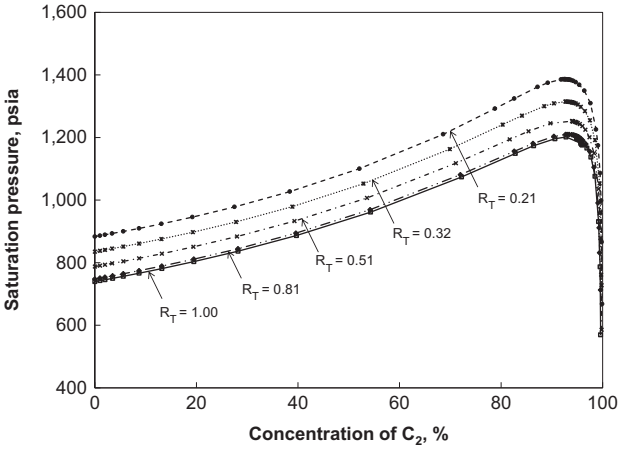

Fig. 14. Saturation pressure predictions for the oil-C_2 mixtures with corrected fluid models with different throughput-ratio (R_T) values from 0.21 to 1.0. The predicted saturation pressures deviate from the original one (R_T of 1.0) as R_T is decreased. Table 2 gives the fluid model parameters used.

Step 3. Adjust the c_{Dh} to match the original oil density and viscosity.
Step 4. Adjust the volume-shift parameters of injected gas components to match the oil recovery at breakthrough (Time 1).
Step 5. Adjust the γ_h index to match the oil recovery between Times 1 and 2.

This algorithm has been used successfully for various cases, part of which will be presented in Section 4.

3.3. Relationship between the adjustment parameters and R_T

The three main adjustment parameters, γ_a, γ_h, and c_{Dh}, exhibit monotonic trends with respect to R_T. Interestingly, applications of the characterization method for various different cases have indicated that their trends are somewhat linear with respect to R_T, when R_T is not close to zero.

To show this, the algorithm is applied to the previously-mentioned DPF with the ternary fluid system, but with different R_T values, 0.21, 0.51, 0.65, and 0.81. Tables 1 and 2 give the simulation conditions and fluid properties used, respectively. Fig. 10 presents that the C_{10} recovery is successfully reproduced by SPF with a corrected fluid model for each of the different R_T's. Fig. 11 shows the resulting values of γ_a, γ_h, and c_{Dh} at different R_T values. Both γ_a and γ_h monotonically decrease with increasing R_T. These adjustment parameters become zero at $R_T = 1$ because there is no need to split the oil components in such a case. The oil density from a corrected fluid model will be greater than the original density when γ_h and γ_a are positive. Therefore, negative values of c_{Dh} are obtained to retain the original oil density when $R_T \neq 1$. Fig. 11 shows that c_{Dh} monotonically increases with increasing R_T, and is zero for R_T of unity. The linear trend lines correlate well the behavior of γ_a, γ_h, and c_{Dh} with respect to R_T in this case.

The adjustment parameters at $R_T = 0$ are estimated by extrapolating the linear trends given in Fig. 11. As mentioned in Section 2.2, R_T of zero corresponds to SPF with the S_{orm} method. Therefore, comparison of the oil recovery from the SPF with these extrapolated parameters to that from the SPF with the S_{orm} method can serve as a severe test of the linear correlations. Fig. 12 shows that at earlier PVIs, the linear extrapolations to R_T of zero give a reasonable representation of the limiting capacitance flow behavior, where the bypassed oil is unrecoverable as in the S_{orm} method. However, they deviate as PVI increases. This is because the extrapolated γ_a index is not high enough to represent immobile components at R_T of zero. Nevertheless, the linear correlations of γ_a, γ_h, and c_{Dh} with respect to R_T are reasonable when R_T is not close to zero (see Fig. 11). Although these linear correlations are purely empirical within this research, the monotonic variations with respect to R_T are qualitatively consistent with the roles of the adjustment parameters in the flow-based fluid characterization method.

Linear correlations of γ_a and γ_h with respect to R_T can be useful; once values for γ_a and γ_h are obtained for a given non-zero R_T by applying the algorithm described in Section 3.2 to the capacitance flow of interest, linear correlations can be established and used for estimating γ_a and γ_h for different R_T values. It is straightforward to determine the corresponding c_{Dh} value for a given set of γ_a and γ_h, since step 3 does not require flow simulations (see Section 3.2). Therefore, although c_{Dh} has also exhibited linear correlations with respect to R_T for the cases tested (e.g., Fig. 11), we consider that the linearity of γ_a and γ_h with respect to R_T is of more fundamental importance.

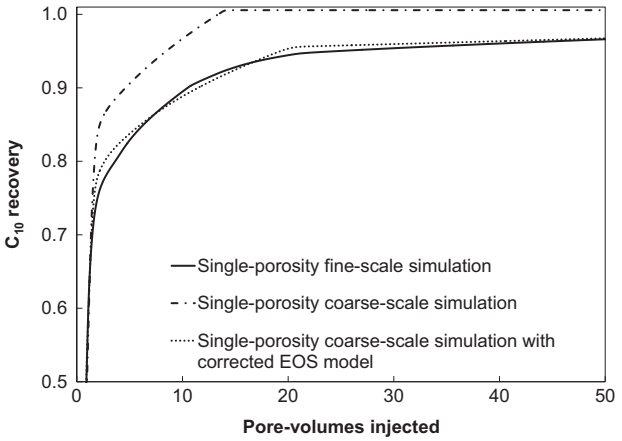

Fig. 15. C_{10} recovery predictions in the areal 2-D heterogeneous reservoir simulations. The recovery prediction from the fine-scale simulation can be reproduced with the coarse-scale simulation when the fluid model is corrected for sub-grid scale capacitance. The coarse-scale simulation erroneously overestimates the oil recovery without correction of the fluid model. Table 2 gives the fluid properties used. The porosity distribution for the fine-scale model is given in Fig. 4.

Table 3
Properties of the Shengli oil.

	Oil (mole fraction)	Gas (mole fraction)	Molecular weight (g/mol)	T_C (°F)	P_C (psia)	ω	Critical volume (ft^3/lb-mol)
N_2	0.003	0.000	28.01	−232.51	492.26	0.0400	1.44
CO_2	0.005	1.000	44.01	87.89	1069.80	0.2250	1.51
C_1	0.244	0.000	16.04	−116.59	667.18	0.0080	1.59
C_2	0.023	0.000	30.07	90.05	708.37	0.0980	2.37
C_3	0.031	0.000	44.10	205.97	615.83	0.1520	3.25
C_4	0.030	0.000	58.12	305.69	551.15	0.1930	4.08
C_5	0.038	0.000	72.15	385.61	489.36	0.2510	4.87
C_6	0.069	0.000	86.18	453.65	430.62	0.2960	5.93
PC1	0.215	0.000	122.99	775.74	510.68	0.1761	10.11
PC2	0.153	0.000	173.09	927.18	406.40	0.2776	11.94
PC3	0.114	0.000	231.28	1056.90	334.17	0.3975	14.6
PC4	0.076	0.000	350.53	1229.94	251.21	0.6096	17.38

3.4. Deviation of compositional phase behavior from the original fluid model

As mentioned in Section 3.1, the deviation of compositional phase behavior from the original fluid model of interest can be suppressed by not adjusting the covolume parameters. Nevertheless, compositional phase behavior is inevitably altered in the flow-based fluid characterization when $\gamma_a \neq 0$. There is no deviation of compositional phase behavior from the original fluid model when $\gamma_a = 0$ at $R_T = 1.0$.

The ternary fluid system is used here again, to show how much deviation of the corrected fluid model from the original model occurs in terms of compositional behavior predictions for different R_T values. Fig. 13 shows two-phase envelopes predicted in *P-T* space for the ternary oil with corrected fluid models at different R_T values. The two-phase envelope becomes greater in *P-T* space with increasing R_T. The original bubble-point pressure is 738.6 psia at 158°F. However, it is increased to 752.6 psia, 785.5 psia, and 887.3 psia at R_T's of 0.81, 0.51, and 0.21, respectively. The respective deviations for these R_T values are +1.9%, +6.0%, and +16.8%.

Fig. 14 presents saturation pressure predictions at 158°F for the pseudo binary of the oil and gas given in Table 2. The saturation pressure becomes systematically higher with decreasing R_T. For example, the saturation pressure for the equimolar pseudo binary mixture is 739.7 psia at $R_T = 1.0$. It is increased to 747.7 psia at R_T of 0.81, 787.7 psia at R_T of 0.51, and 883.4 psia at R_T of 0.21. The corresponding deviation is +1.1% at R_T of 0.81, +6.5% at R_T of 0.51, and +19.4% at R_T of 0.21. However, this level of deviation of compositional phase behavior predictions from experimental data is often observed when a cubic EOS with the van der Waals mixing rules is used with a fixed set of binary interaction parameters [for example, see Kumar and Okuno (2012) for nine different binary mixtures C_1–C_{16}, C_1–C_{20}, C_2–C_{16}, C_2–C_{20}, C_2–C_{22}, C_2–C_{24}, C_6–C_{16}, C_6–C_{24}, and C_6–C_{36}].

The MMP is calculated to be 1174.2 psia at 158°F for the original oil and gas properties given in Table 2. The MMP is 1180.9 psia at R_T of 0.81, 1214.4 psia at R_T of 0.51, and 1303.4 psia at R_T of 0.21. The corresponding deviation is +0.6% at R_T of 0.81, +3.4% at R_T of 0.51, and +11.0% at R_T of 0.21. The deviations may be within or similar to the level of uncertainties inherent to reservoir oil characterization using an EOS, depending on the level of capacitance, or R_T.

Table 4
Reservoir properties for 1-D SPF simulation of the Shengli oil core flood.

Dimensions	$0.0123 \times 0.8723 \times 0.8723$ in^3
Number of gird blocks	$500 \times 1 \times 1$
Porosity	0.1529
Permeability	19.49 md (*X*, *Y*, *Z*)
Reservoir pressure	2842.65/3263.36/3727.48 psia
Reservoir temperature	258.80°F
Injection rate	4.39 in^3/min
Production pressure	2842.65/3263.35/3727.48 psia
Relative permeability model	Corey
Residual saturation (Oil/Gas)	0.1/0.0
Endpoint relative permeability (Oil/Gas)	1.0/0.5
Exponent (Oil/Gas)	1.5/3.0
Initial saturation (Oil/Gas)	1.0/0.0

3.5. Representation of capacitance flow behavior observed in the fine-scale simulation

In Section 2.3, capacitance flow behavior was explained by use of a fine-scale simulation. A coarse-scale DPF simulation was then fitted successfully to the fine-scale simulation results. This subsection shows the application of the flow-based fluid characterization method for representing this capacitance flow behavior by use of efficient SPF simulation. Fine-scale simulation case 3 is considered. The DPF model fitted to case 3 resulted in the bypassed fraction of 0.08 and the throughput ratio of 0.14 (see Fig. 8). These dimensionless numbers indicate the importance of properly modeling capacitance flow behavior in this case.

The flow-based fluid characterization method results in an estimated value of 0.487 for γ_a, 0.3125 for γ_h, and −0.09 for c_{Dh}. The resulting oil recovery prediction is compared with the original fine-scale simulation in Fig. 15. The SPF simulation with the corrected fluid model exhibits accurate representation of the capacitance flow behavior. It is not possible to reproduce the oil recovery using SPF if the flow-based fluid characterization method is not used.

4. Case studies

Sections 2.3 and 3.5 showed that capacitance flow behavior in a fine-scale simulation can be efficiently reproduced by the following two steps:

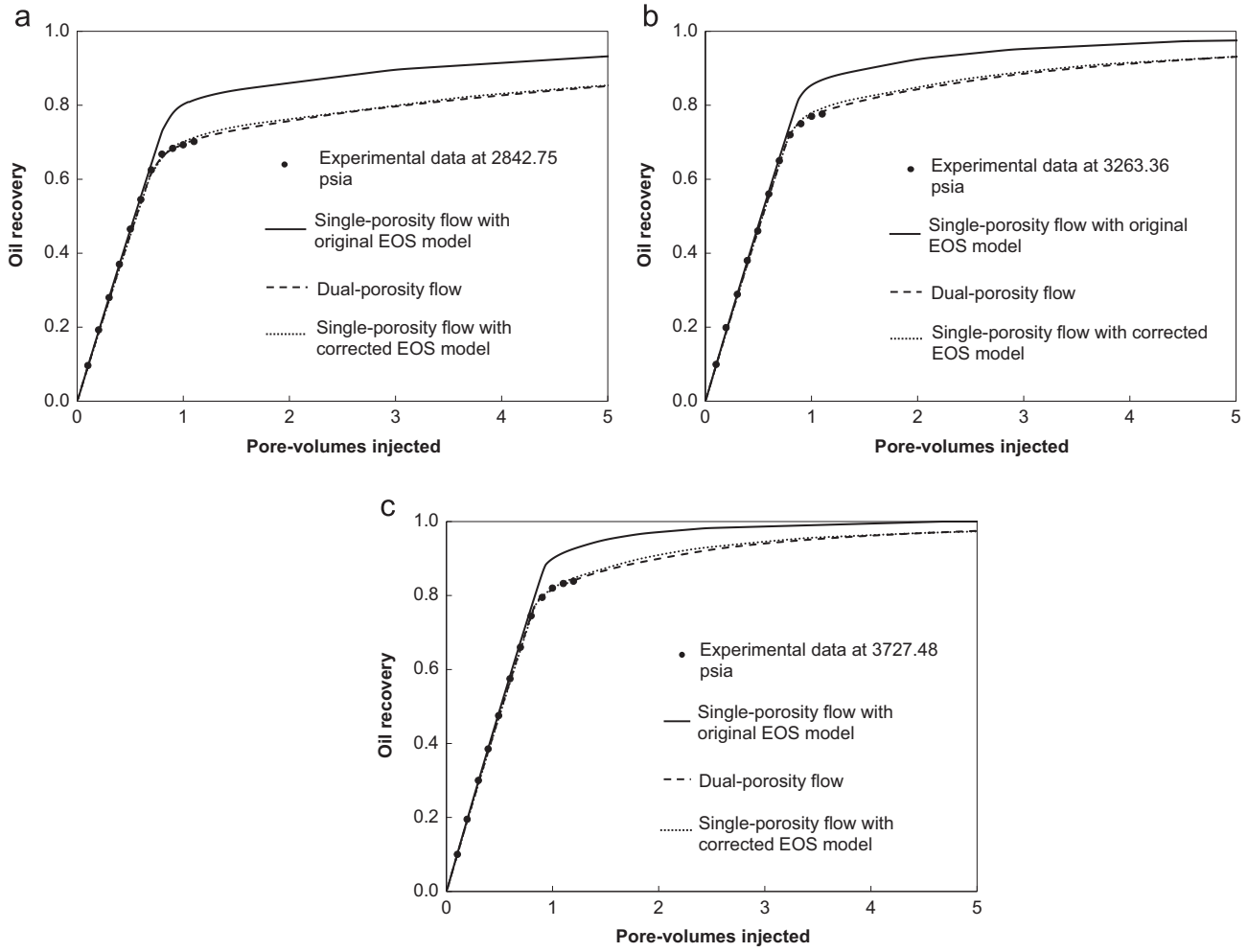

Fig. 16. 1-D DPF models fitted to core-flood data for the Shengli oil. (a) Bypassed fraction is 0.18 and throughput ratio is 0.48 at 2842.75 psia, (b) Bypassed fraction is 0.14 and throughput ratio is 0.48 at 3263.36 psia, and (c) Bypassed fraction is 0.14 and throughput ratio is 0.472 at 3727.48 psia. The recovery predictions from 1-D SPF simulations cannot reproduce the core-flood data unless the fluid model is corrected for capacitance. The fluid model characterized for 3263.36 psia is successfully applied at the other two pressures since the flow characteristics represented by the bypassed fraction and throughput ratio are similar to one another.

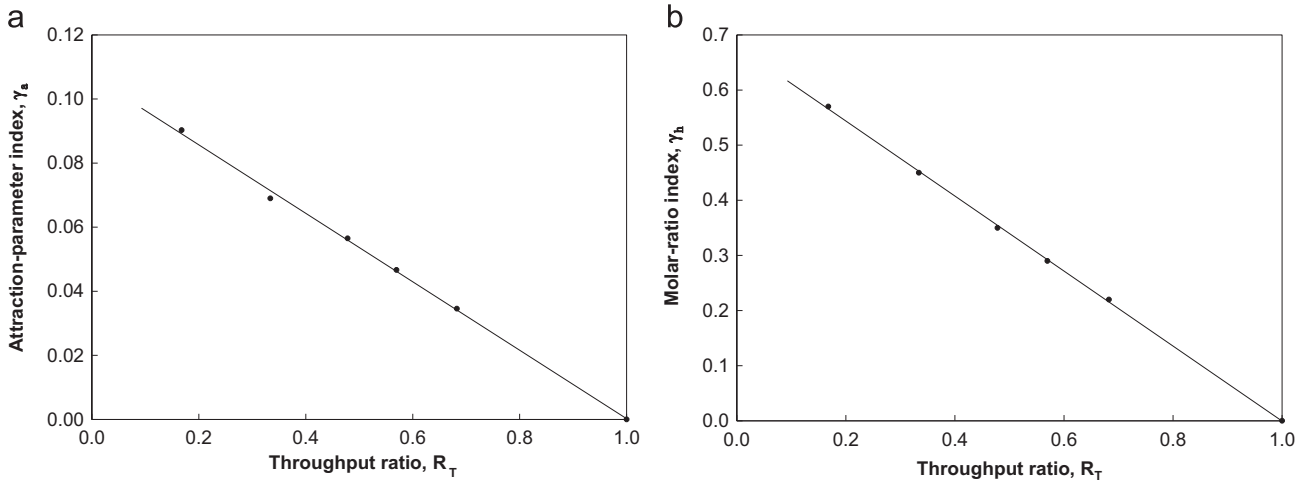

Fig. 17. Empirical linear relationship observed for the attraction-parameter index γ_a and the molar-ratio index γ_h with respect to R_T at 3263.36 psia. The core flooding case is at R_T of 0.48.

Step 1. Quantification of capacitance flow behavior by fitting a coarse-scale DPF model to the oil recovery from a fine-scale simulation. This gives certain values for bypassed fraction and throughput ratio (R_T^*).

Step 2. Correction of the original fluid model for capacitance using the flow-based fluid characterization method. The coarse-scale DPF model is reduced to the corresponding SPF model with a corrected fluid model.

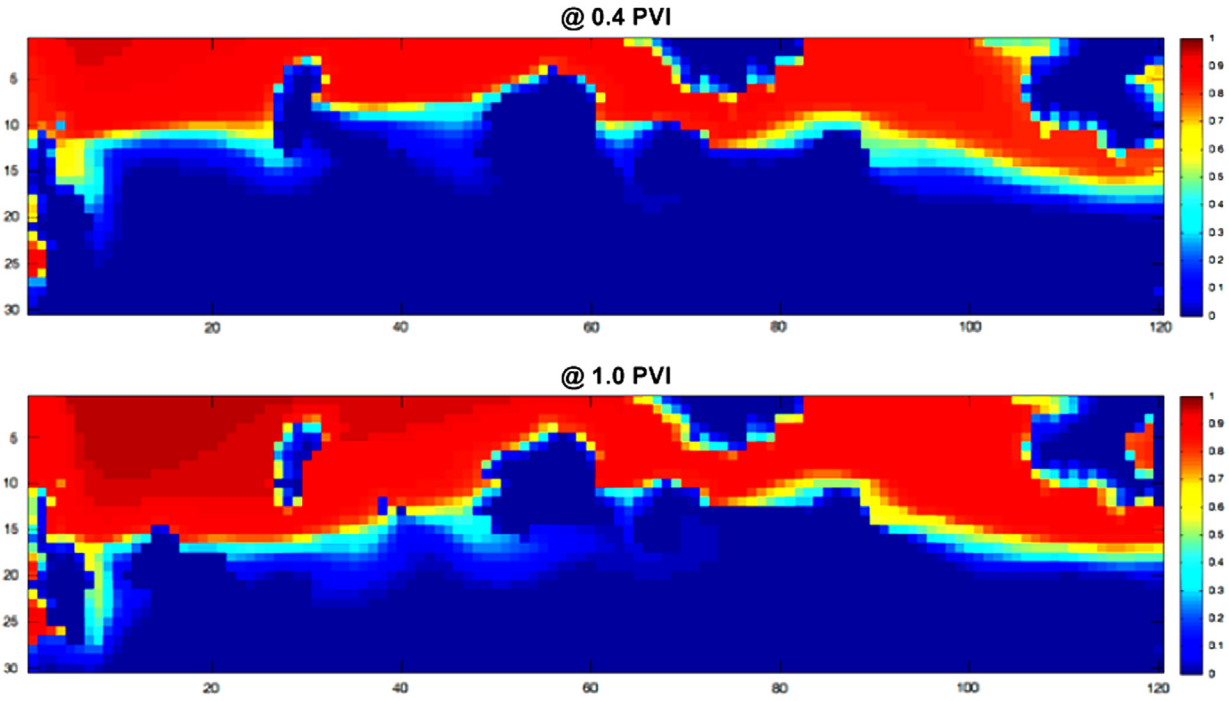

Fig. 18. CO_2 concentration distributions in the vertical 2-D fine-scale simulation at 0.4 PVI and 1.0 PVI. The channeling flow under gravity is observed. Table 3 gives the fluid properties used. The porosity distribution given in Fig. 4 was used in the vertical two dimensions.

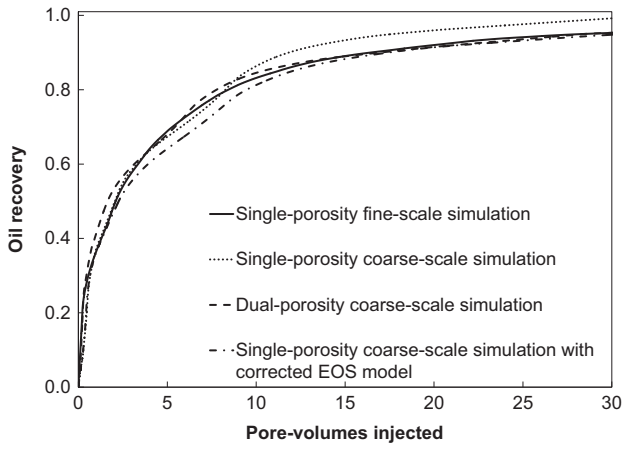

Fig. 19. Oil recovery predictions for the vertical 2-D case. The DPF simulation successfully represents the capacitance flow behavior with a bypassed fraction of 0.10 and a throughput ratio of 0.22. The SPF simulation with a corrected fluid model is then used to reproduce the capacitance flow, which cannot be modeled using the coarse-scale SPF simulation. Table 3 gives the fluid properties used. The porosity distribution given in Fig. 4 was used in the vertical two dimensions.

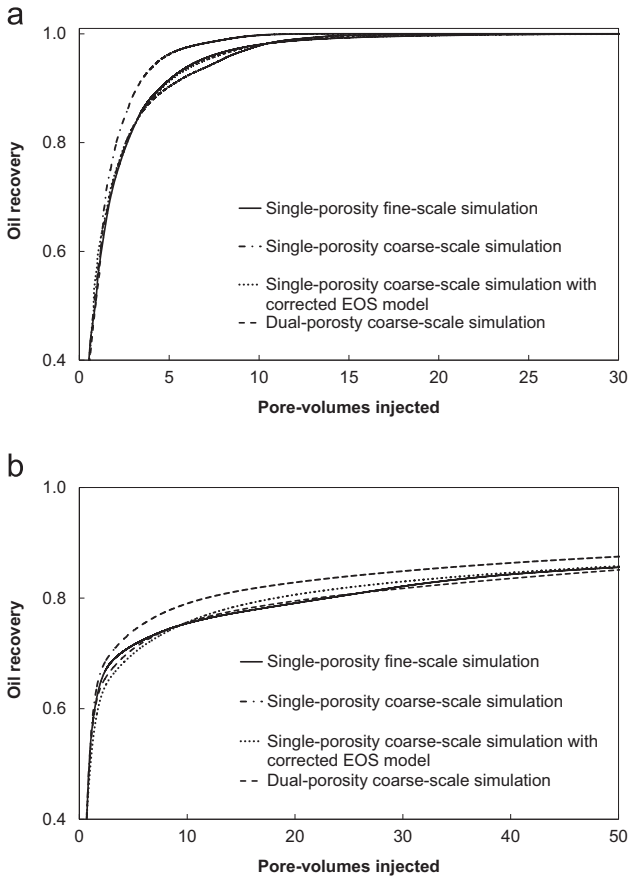

Fig. 20. Oil recovery predictions for two layers from the SPE-10 problem. (a) Layer 15. $B=0.10$, $R_T=0.52$, $\gamma_a=0.223$, $\gamma_h=0.32$, and $c_{Dh}=-0.14$. (b) Layer 80. $B=0.05$, $R_T=0.51$, $\gamma_a=0.364$, $\gamma_h=0.28$, and $c_{Dh}=-0.24$.

For different R_T values anticipated in a specific application, the SPF model from Step 2 can be used with another fluid model that is based on linear correlations of γ_a, γ_h, and c_{Dh} with respect to R_T between 1.0 and R_T^* (extrapolated if necessary).

This section presents case studies for capacitance flow in core floods and fine-scale simulations for the Shengli oil with CO_2, and layers 15 and 80 from the SPE-10 problem (Christie and Blunt, 2001). The two-step method is applied for efficient representation of capacitance flow by use of SPF with a corrected fluid model.

4.1. Core floods

Ren et al. (2011) conducted core floods of the Shengli oil by CO_2 at 258.8°F. Details of the core-flooding apparatus and core properties are given in Ren et al. (2011). The MMP measured at the reservoir temperature 258.8°F was 3800 psia. Table 3 gives the EOS fluid model developed based on the data given in Ren et al.

(2011) and the characterization method of Kumar and Okuno (2013). Ren et al. (2011) described that the reservoir pressure dropped below the MMP after depletion in the G89 block of the Shengli oil field. Hence, the injection pressures tested in their core floods were set below the MMP in order to determine an optimal injection pressure.

In this research, a 1-D SPF model was first made as given in Table 4. The numerical Péclet number is estimated to be approximately 660 with uniform 500 grid blocks and 0.01-hour time step with the fully implicit scheme. The recovery predictions at three different pressures, 2842.65 psia, 3263.36 psia, and 3727.48 psia, were erroneously higher than the experimental results of Ren et al. (2011), as shown in Fig. 16. This is because the sub-grid scale capacitance flow behavior could not be captured in the 1-D SPF simulations with the conventional local equilibrium assumption. The two-step method is applied to these core-flooding data below.

The first step is to quantify the capacitance flow behavior using the 1-D DPF model. Fig. 16 shows that the 1-D DPF model is fitted well to the core-flooding data (black dots) at three different pressures. The resulting dimensionless groups associated with capacitance (B, R_T) are (0.18, 0.48) at 2842.75 psia, (0.14, 0.48) at 3263.36 psia, and (0.14, 0.472) at 3727.48 psia, where B and R_T are the bypassed fraction and throughput ratio, respectively.

In the second step, the flow-based fluid characterization method is applied with the DPF at 3263.36 psia. Fig. 16(b) shows that the SPF with a corrected fluid model can reproduce the oil recovery predictions from the DPF. The resulting dimensionless groups associated with capacitance (γ_a, γ_h) are (0.12, 0.36), where γ_a and γ_h are the attraction-parameter index (Eq. (10)) and the molar-ratio index (Eq. (11)), respectively. The corresponding c_{Dh} is calculated to be -0.06. Since the levels of capacitance measured by B and R_T are similar at the three pressures, the corrected fluid model for 3263.36 psia is applied to the other pressures, 2842.75 psia and 3727.48 psia. Fig. 16 (a and c) shows that the resulting SPF simulations are still in good agreement with the corresponding DPF simulations and experimental results.

To see the relationship of γ_a and γ_h with R_T, four more cases are generated with the DPF at different R_T's. Each of the DPF cases is reproduced by the corresponding SPF based on step 2, the flow-based fluid characterization method. Fig. 17 shows the resulting values of γ_a and γ_h for the five R_T values, including R_T of 0.48. They are correlated well with straight lines that go through zero at R_T of 1.0.

4.2. Vertical 2-D fine-scale simulation

Capacitance flow behavior observed in vertical 2-D fine-scale simulations is considered in this subsection. The porosity and permeability distributions used are the same as those in Section 2.3 (see Fig. 4), except that the original y direction is changed to the z (vertical) direction. The fluid properties used are given in Table 3; that is, the injection gas is pure CO_2. The reservoir pressure and temperature are 3263.36 psia and 258.8°F, respectively.

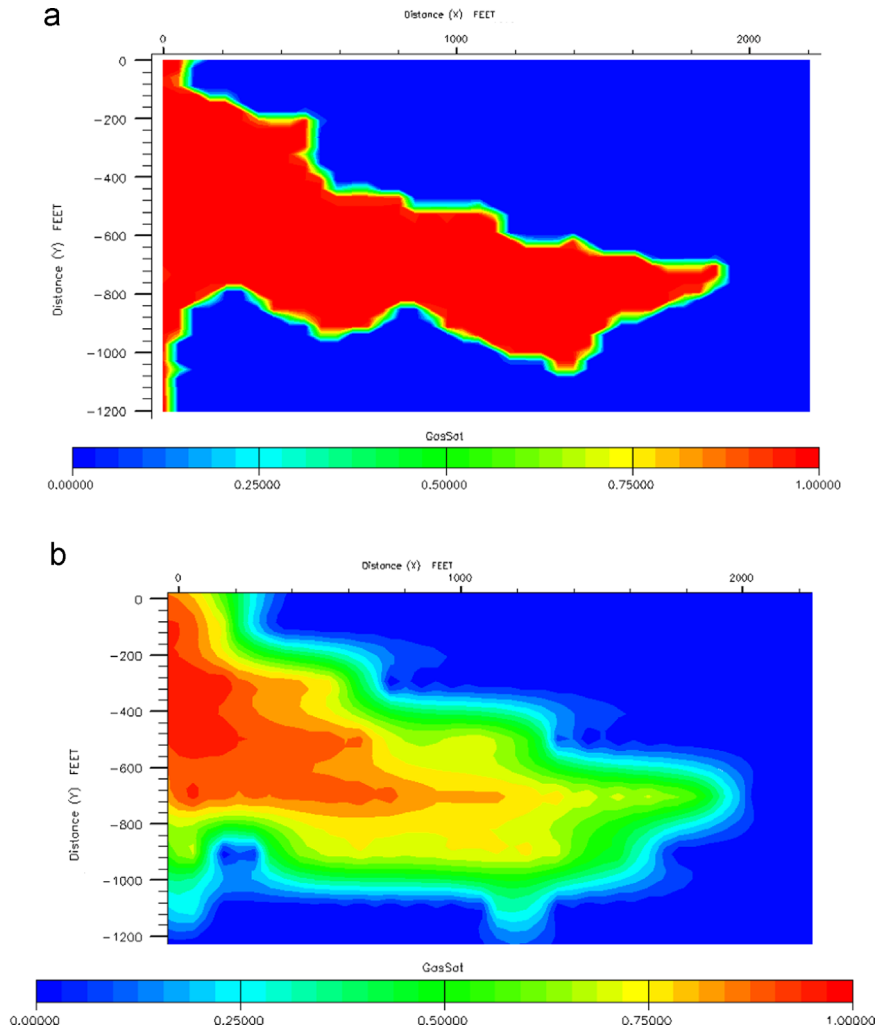

Fig. 21. Gas saturation contours at 0.74 PVI for layer 15 of the SPE-10 problem. (a) Original fine-scale simulation. (b) Coarse-scale simulation with the corrected fluid model. The root-mean-square deviation is 15.3%.

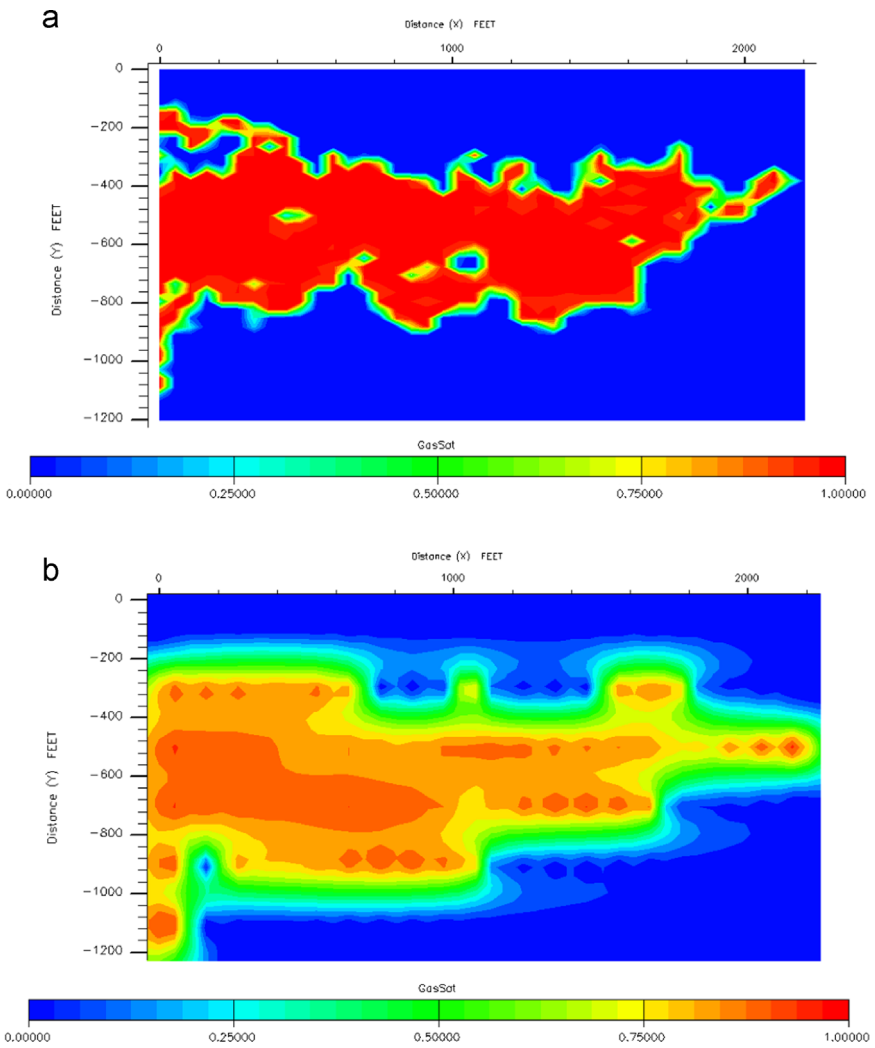

Fig. 22. Gas saturation contours at 0.98 PVI for layer 80 of the SPE-10 problem. (a) Original fine-scale simulation. (b) Coarse-scale simulation with the corrected fluid model. The root-mean-square deviation is 29.5%.

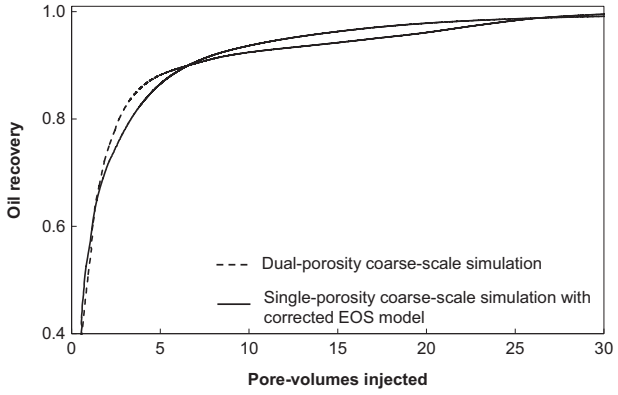

Fig. 23. Oil recovery predictions for layer 15 of the SPE-10 problem. B=0.10 and R_T=0.33. The prediction from the linearly extrapolated SPF is in good agreement with the benchmark result from the DPF. The extrapolation gives (γ_a, γ_h, c_{Dh})= (0.314, 0.45, –0.20) at R_T=0.33.

Fig. 18 illustrates the CO_2 concentration distributions in the vertical 2-D fine-scale simulation at 0.4 PVI and 1.0 PVI. The channeling flow under gravity is clearly observed. In the first step, the original 120×30 grid blocks are upscaled to 12×3 coarse-scale grid blocks. The coarse-scale DPF model is fitted to the fine-scale simulation in terms of oil recovery, resulting in a bypassed fraction of 0.10 and a R_T of 0.22 (Fig. 19). In step 2, the flow-based fluid characterization method is used to fit the coarse-scale SPF to the coarse-scale DPF, resulting in γ_a of 0.21, γ_h of 0.12, and c_{Dh} of -0.1. As shown in Fig. 19, the oil recovery predictions at later PVIs from the fine-scale simulation can be quantitatively reproduced by use of the coarse-scale SPF with the corrected fluid model.

4.3. Layers 15 and 80 from SPE 10

In this subsection, the proposed two-step method is applied for upscaling of layers 15 and 80 from the SPE-10 problem (Christie and Blunt, 2001), in which methane is injected to displace the reservoir oil consisting of methane, CO_2, n-C_4, and C_{10} at 211.73° F. It is a partially miscible displacement. For each of the layers, the original fine-scale model of $220 \times 60 \times 1$ is upscaled to a coarse-scale model of $22 \times 6 \times 1$; i.e., the upscaling ratio is 100. These upscaling cases were used by Salehi et al. (2013) to demonstrate the applicability of their compositional upscaling method. The simulation conditions can be found in Christie and Blunt (2001) and Salehi et al. (2013), and are not duplicated here.

Quantification of the capacitance flow yields the DPF parameters (B, R_T) of (0.10, 0.52) for layer 15, and (0.05, 0.51) for layer 80. Then, the resulting fluid-characterization parameters (γ_a, γ_h, c_{Dh}) are (0.223, 0.32, –0.14) for layer 15, and (0.364, 0.28, –0.24) for layer 80. Fig. 20 shows oil recoveries from four different simulation runs

for each layer; i.e., the original fine-scale simulation, SPF with the original fluid model, DPF, and SPF with the corrected fluid model. In the DPF simulation and the SPF simulation with the corrected fluid model, the capacitance flow behavior that is present in the original fine-scale model is properly represented for each layer. This figure indicates that layer 15 is more challenging for the flow-based fluid characterization because the SPF with the original fluid model gives greater absolute deviations from the original fine-scale simulation in terms of oil recovery.

It was observed that the coarse-scale SPF with the corrected fluid model requires much less computational time than the original fine-scale simulation; e.g., it takes less than 2% of the total computational time taken by the fine-scale simulation for layer 15. For layer 80, the computational-time ratio is less than 1%. Similar levels of computational efficiency were achieved by Salehi et al. (2013) with their upscaling method.

Fig. 21 shows gas saturation contours in the original fine-scale simulation and the coarse-scale simulation with the corrected fluid model for layer 15 at 0.74 PVI (390 days). Gas saturation contours for layer 80 at 0.98 PVI (130 days) are given in Fig. 22. The root-mean-square deviation in gas saturation is calculated to be 15.3% for Fig. 21, and 29.5% for Fig. 22. Salehi et al. (2013) presented that their upscaling method resulted in the deviation of 8.3% for layer 15 at 390 days, and 10.2% for layer 80 at 130 days. Hence, the method of Salehi et al. (2013) exhibited higher accuracy for upscaling of the two layers at the tested PVI. This is expected because their method allows for local adjustment of compositional flow.

For layer 15, which is more challenging than the other layer, the applicability of linear extrapolations of γ_a, γ_h, and c_{Dh} are examined. They are extrapolated to a R_T value of 0.33 to obtain $(\gamma_a, \gamma_h, c_{Dh})=(0.314, 0.45, -0.20)$, on the basis of the linear correlations from the original case with $(R_T, \gamma_a, \gamma_h, c_{Dh})=(0.52, 0.223, 0.32, -0.14)$. Fig. 23 shows that the linearly extrapolated SPF is in good agreement with the DPF with (B, R_T) of (0.10, 0.33).

Unlike in local-upscaling methods, it is not the primary objective to reproduce local saturations/concentrations in the proposed two-step method. In the global upscaling method developed in the current paper, local saturations/concentrations are approximated indirectly by matching global flow behavior under capacitance. Nevertheless, the simplicity of the method developed in this research gives the following distinct features: (1) it can quantify the level of capacitance flow behavior observed in a flow experiment or fine-scale simulation in a simple, but physically meaningful manner by use of DPF with B and R_T; (2) it can represent the quantified capacitance flow in coarse-scale SPF in a simple, systematic manner with no change in the conventional compositional-flow formulation. The simplicity owing to the selected parameters resulted in the finding that γ_a, γ_h, and c_{Dh} have empirically linear correlations with R_T.

5. Conclusions

This paper presented capacitance flow behavior in compositional reservoir simulation. The two-step method was proposed to efficiently reflect in coarse-scale single-porosity simulation the capacitance flow behavior observed in core floods and fine-scale simulations. Conclusions are as follows:

1. Dual-porosity flow (DPF) can capture the characteristics of capacitance flow behavior. Quantification of the capacitance is possible with bypassed fraction and throughput ratio (R_T). R_T is defined as the ratio of throughput required for ultimate oil recovery without intra-block mass flux to that with intra-block mass flux. R_T of zero corresponds to single-porosity flow (SPF) with the S_{orm} method. R_T of unity corresponds to the traditional SPF with the local equilibrium assumption.
2. In the flow-based fluid characterization method developed in this research, the fluid model of interest is corrected for capacitance. It adjusts in-situ propagation rates of components through the attraction parameters. Two main adjustment parameters are the attraction-parameter index (γ_a defined by Eq. (10)) and the molar-ratio index (γ_h defined by Eq. (11)). These adjustment parameters decrease monotonically with increasing R_T. In the cases studied, they are well correlated with R_T using straight lines that go through zero at R_T of 1.0, where the fluid model naturally becomes the original one (i.e., no capacitance).
3. The two-step method presented requires no change in the governing equations in compositional reservoir simulation. It can be easily applied with the existing reservoir simulators.

Acknowledgments

Research grants from the Natural Sciences and Engineering Research Council of Canada (RGPIN 418266) and Japan Petroleum Exploration Co., Ltd. are gratefully acknowledged.

References

Al-Wahaibi, Y.M., Muggeridge, A.H., Grattoni, C.A., 2007. Experimental and numerical studies of gas/oil multicontact miscible displacements in homogeneous and crossbedded porous media. SPE J. 12 (1), 62–76.
Aronofsky, J.S., Heller, J.P., 1957. A diffusion model to explain mixing of flowing miscible fluids in porous media. Pet. Trans. AIME 210, 345–349.
Bahralolom, I., Bretz, R.E., Orr Jr., F.M., 1988. Experimental investigation of the interaction of phase behavior with microscopic heterogeneity in a CO_2 flood. SPE Reserv. Eng. 3 (2), 662–672.
Ballin, P.R., Clifford, P.J., Christie, M.A., 2002. Cupiagua, modeling of a complex fractured reservoir using compositional upscaling. SPE Reserv. Eval. Eng. 5 (6), 488–498.
Bardon, C., Longeron D.G., Baudoin F., Delhomme, A., Naili, N. 1994. Gas/oil relative permeabilities and residual oil saturations in a field case of a very light oil, in the near-miscibility conditions. In: Paper SPE 28625 presented at the SPE Annual Technical Conference and Exhibition, New Orleans, Louisiana, September 25–28.
Barker, J.W., Evans, S.C., 1995. Predictive model for viscous fingering in compositional WAG floods. SPE Reserv. Eng. 10 (2), 116–122.
Barker, J.W., Fayers, F.J., 1994. Transport coefficients for compositional simulation with coarse grids in heterogeneous media. SPE Adv. Technol. Ser. 2 (2), 103–112.
Barker, J.W., Prevost, M., Pitrat, E. 2005. Simulating residual oil saturation in miscible gas flooding using alpha-factors. In: Paper SPE 93333 presented at the SPE Reservoir Simulation Symposium, The Woodlands, Texas, USA, January 31–February 2.
Barker, L.E., 1977. Effects of dispersion and dead-end pore volume in miscible flooding. SPE J. 17 (3), 219–227.
Blunt, M., Christie, M., 1994. Theory of viscous fingering in two phase, three component flow. SPE Adv. Technol. Ser. 2 (2), 52–60.
Bourgeois, M.J., Thibeau, S., Guo, J. 2011. Modeling residual oil saturation in miscible and immiscible gas floods by use of alpha-factors. In: Paper SPE 143379 presented at the SPE EUROPEC/EAGE Annual Conference and Exhibition in Vienna, Austria, May 23–26.
Bourgeois, M.J., Gommard, D.R., Gouas, H. 2012. Simulating early gas breakthrough in undersaturated oil using alpha-factors. In: Paper SPE 161460 presented at the Abu Dhabi international Petroleum Exhibition and Conference, Abu Dhabi, UAE, November 11–14.
Brock, D.C., and Orr Jr., F.M. 1991. Flow Visualization of Viscous Fingering in Heterogeneous Porous Media. Paper SPE 22614 presented at SPE Annual Technical Conference and Exhibition held in Dallas, TX, October 6-9.
Brown, J.S., Al-Kobaisi, M.S. and Kazemi, H. 2013. Compositional phase trapping in CO_2 WAG simulation. In: Paper SPE 165983 presented at the SPE Reservoir Characterization and Simulation Conference and Exhibition, Abu Dhabi, UAE, September 16–18.
Burger, J.E., Mohanty, K.K., 1997. Mass transfer from bypassed zones during gas injection. SPE Reserv Eng 12 (2), 124–130.
Burger, J.E., Bhogeswara, R., Mohanty, K.K., 1994. Effect of phase behavior on bypassing in enriched gasfloods. SPE Reserv Eng 9 (2), 112–118.
Burger, J.E., Springate, G.S., Mohanty, K.K., 1996. Experiments on bypassing during gasfloods in heterogeneous porous media. SPE Reserv Eng 11 (2), 109–115.

Campbell, B.T., Orr Jr., F.M., 1985. Flow visualization for CO_2/crude-oil displacements. SPE J. 25 (5), 665–678.
Camy, J.P. and Emanuel, A.S. 1977. Effect of grid size in the compositional simulation of CO_2 injection. In: Paper SPE 6894 presented at 52nd Annual Technical Conference and Exhibition of the SPE, Denver, October 9–12.
Cao, H., 2002. Development of Techniques for General Purpose Simulators. Ph.D. dissertation. Stanford University, Stanford, CA.
Chang, Y.-B., Pope, G.A., Sepehrnoori, K., 1990. A higher-order finite-difference compositional simulator. J. Pet. Sci. Eng. 5 (1), 35–50.
Chatzis, I., Norman, M.R., Hau, L.T., 1983. Magnitude and detailed structure of residual oil saturation. SPE J. 23 (2), 311–326.
Christie, M.A., Blunt, M.J., 2001. Tenth SPE comparative solution project: a comparison of upscaling techniques. SPE Reserv. Eval. Eng. 4 (4), 308–317.
Christie, M.A., Clifford, P.J., 1998. Fast procedure for upscaling compositional simulation. SPE J. 3 (3), 272–278.
Cinar, Y., Jessen, K., Berenblyum, R., Juanes, R., Orr Jr., F.M., 2006. An experimental and numerical investigation of crossflow effects in two-phase displacements. SPE J. 11 (2), 216–226.
Coats, K., 1980. An equation of state compositional model. SPE J. 20 (5), 363–376.
Coats, K.H., Smith, B.D., 1964. Dead-end pore volume and dispersion in porous media. SPE J. 4 (1), 73–84.
Coats, K.H., Thomas, L.K., Pierson, R.G., 2007. Simulation of miscible flow including bypassed oil and dispersion control. SPE Reserv. Eval. Eng. 10 (5), 500–507.
Collins, D.A., Nghiem, L.X., Li, Y.-K., Grabonstotter, J.E., 1992. An efficient approach to adaptive-implicit compositional simulation with an equation of state. SPE Reserv. Eng. 7 (2), 259–264.
Dai, K.K., Orr Jr., F.M., 1987. Prediction of CO_2 flood performance: interaction of phase behavior with microscopic pore structure heterogeneity. SPE Reserv. Eng. 2 (4), 531–542.
Deans, H.A., 1963. A mathematical model for dispersion in the direction of flow in porous media. SPE J. 3 (1), 49–52.
Dindoruk, B., 1992. Analytical Theory of Multiphase, Multicomponent Displacement in Porous Media Ph.D. dissertation. Stanford University, Stanford, CA.
Eclipse 300, 2010. Schlumberger.
Fayers, F.J., Barker, J.W., Newley, T.M.J., 1989. Effects of heterogeneities on Phase Behavior in Enhanced Oil Recovery, The Mathematics of Oil Recovery. Clarendon Press, Oxford, UK, pp. 115–150.
Fayers, F.J., Blunt, M.J, Christie, M.A., 1992. Comparisons of empirical viscous-fingering models and their calibration for heterogeneous problems. SPE Reserv. Eng. 7 (2), 195–203.
Gardner, J.W., Ypma, J.G.J., 1984. An investigation of phase-behavior/macroscopic-bypassing interaction in CO_2 flooding. SPE J. 24 (5), 508–520.
Hill, R., 1963. Elastic properties of reinforced solids: Some theoretical principles. J. Mech. Phys. Solids 11 (5), 357–372.
Hiraiwa, T., Suzuki, K., 2007. New method of incorporating immobile and non-vaporizing residual oil saturation into compositional reservoir simulation of gasflooding. SPE Reserv. Eval. Eng. 10 (1), 60–65.
Iranshahr, A., Chen, Y., Voskov, D.V., 2014. A coarse-scale compositional model. Comput. Geosci. 18 (5), 797–815.
Johns, R.T., 1992. Analytical Theory of Multicomponent Gas Drives with Two-Phase Mass Transfer Ph.D. dissertation. Stanford University, Stanford, CA.
Khosravi, M., Alireza, B., Emadi, M., Rostami, B., Roayaie, E., 2014. Mechanistic investigation of bypassed-oil recovery during CO_2 injection in matrix and fracture. Fuel 117 (A), 43–49.
Koval, E.J., 1963. A method for predicting the performance of unstable miscible displacement in heterogeneous media. SPE J. 3 (2), 145–154.
Kumar, A., Okuno, R., 2012. Critical parameters optimized for accurate phase behavior modeling for heavy n-Alkanes up to C_{100} using the Peng-Robinson equation of state. Fluid Phase Equilibria 335, 46–59.
Kumar, A., Okuno, R., 2013. Characterization of reservoir fluids using an EOS based on perturbation from n-Alkanes. Fluid Phase Equilibria 358, 250–271.
Lake, L.W., 1989. Enhanced Oil Recovery. Prentice Hall Incorporated, United States.
Lange, E.A., 1998. Correlation and prediction of residual oil saturation for gas injection EOR processes. SPE Reserv. Eval. Eng. 1 (2), 127–133.
Lantz, R.B., 1971. Quantitative evaluation of numerical diffusion (Truncation Error). SPE J. 11 (3), 315–320.
Leung, J.Y., Srinivasan, S., 2011. Analysis of uncertainty introduced by scaleup of reservoir attributes and flow response in heterogeneous reservoirs. SPE J. 16 (3), 713–724.
Leung, J.Y., Srinivasan, S., 2012. Scale-up of mass transfer and recovery performance in heterogeneous reservoirs. J. Pet. Sci. Eng. 86–87, 71–86.
Lizuka, R., Al-Shehhi, H.R., Al-Hammadi H.M. 2012. Derivation of immobile and non-vaporizing residual oil saturation under miscible flood from CO_2 coreflood experiments. In: Paper SPE 161568 Abu Dhabi International Petroleum Conference and Exhibition, Abu Dhabi, UAE, November 11–14.
Lohrenz, J., Bray, B.C., Clark, C.R., 1964. Calculating viscosities of reservoir fluids from their compositions. J. Pet. Technol. 16 (10), 1171–1176.
McGuire, P.L., Spence, A.P., Stalkup, F.I., Cooley, M.W., 1995. Core acquisition and analysis for optimization of the prudhoe bay miscible-gas project. SPE Reserv. Eng. 10 (2), 94–100.
Mohanty, K.K., Johnson, S.W., 1993. Interpretation of laboratory gasfloods with multidimensional compositional modeling. SPE Reserv. Eng. 8 (1), 59–66.
Nghiem, L.X., Sammon, P.H. 1997. A non-equilibrium equation of state compositional simulator. In: Paper SPE 37980 presented at Reservoir Simulation Symposium, Dallas, USA, June 8–11.
Nguyen, Q.P., Rossen, W.R., Zitha, P.L.J., Currie, P.K., 2009. Determination of gas trapping with foam using X-ray computed tomography and effluent analysis. SPE J. 14 (2), 222–236.
Orr Jr., F.M., 2007. Theory of Gas Injection Processes. Tie-Line Publications, Holte, Denmark.
PVTsim, 20.0, 2011. Calsep A/S, Lyngby, Denmark.
Pande, K.K. 1992. Effects of gravity and viscous crossflow on hydrocarbon miscible flood performance in heterogeneous reservoirs. In: Paper SPE 24935 presented at SPE Annual Technical Conference and Exhibition held in Washington, D.C. October 4–7.
Pande, K.K., Orr Jr., F.M., 1994a. Effect of viscous crossflow on miscibility development in a two-layer flow system: Part I—ternary vaporizing gas drives. SPE Adv. Technol. Ser. 2 (2), 7–16.
Pande, K.K., Orr Jr., F.M., 1994b. Effect of viscous crossflow on miscibility development in a two-layer flow system: part II—ternary condensing gas drives. SPE Adv. Technol. Ser. 2 (2), 17–25.
Peng, D.Y., Robinson, D.B., 1976. A new two-constant equation of state. Ind. Eng. Chem. Fundam. 15 (1), 59–64.
Peng, X., Du, Z., Liang, B., Qi, Z., 2009. Darcy-stokes streamline simulation for the tahe-fractured reservoir with cavities. SPE J. 14 (3), 543–552.
Ren, Bo, Xu,Yang., Niu, Baolun., Ren, Shaoran., Li, Xiangliang., Li, Pingguo, Song, Xinwang, 2011. Laboratory assessment and field pilot of near miscible CO_2 injection for IOR and storage in a tight oil reservoir of ShengLi Oilfield China. In: Paper SPE 144108 presented at the SPE Enhanced Oil Recovery Conference, Kuala Lumpur, Malaysia, July 19–21.
S-GeMS V2.1, Standford University, Standford, CA.
Salehi, A., Voskov D.V., Tchelepi H.A. 2013. Thermodynamically consistent transport coefficients for upscaling of compositional processes. In: Paper SPE 163576 presented at SPE Reservoir Simulation Symposium, the Woodlands, Texas, USA, February 18–20.
Salter, S.J., Mohanty, K.K. 1982. Multiphase flow in porous media: I. Macroscopic observations and modeling. In: Paper SPE 11017 presented at the SPE Annual Technical Conference and Exhibition, New Orleans, Louisiana, September 26–29.
Shelton, J.L., Schneider, F.N., 1975. The effects of water injection on miscible flooding methods using hydrocarbons and carbon dioxide. SPE J. 15 (3), 217–226.
Smith, D.H., Jikich, S.A. 1994. Characterization of trapped gas saturation and heterogeneity in core samples using miscible-displacement experiments. In: Paper SPE 29161 presented at the SPE Eastern Regional Conference & Exhibition held in Charleston, WV, USA, November 8–10.
Spence Jr., Andrew, P., Watkins R.W. 1980. The effect of microscopic core heterogeneity on miscible flood residual oil saturation. In: Paper SPE 9229 presented at SPE Annual Technical Conference and Exhibition held in Dallas, TX, September 21–24.
Stalkup, F.I., 1970. Displacement of oil by solvent at high water saturation. SPE J. 10 (4), 337–348.
Stern D. 1991. Mechanisms of miscible oil recovery: effects of pore-level fluid distribution. In: Paper SPE 22652 presented at 66th Annual Technical Conference and Exhibition of the Society of Petroleum Engineers held in Dallas, TX, October 6–9.
Todd, M.R., Longstaff, W.J., 1972. The development, testing, and application of a numerical simulator for predicting miscible flood performance. J. Pet. Technol. 24 (7), 874–882.
Watts, J.W., 1986. A compositional formulation of the pressure and saturation equations. SPE Reserv. Eng. 1 (3), 243–252.
Wilke, C.R., Chang, P., 1955. Correlation of diffusion coefficients in dilute solutions. AIChE Journal 1 (2), 364–270.
Wylie, P., Mohanty, K.K., 1997. Effect of water saturation on oil recovery by near-miscible gas injection. SPE Reserv. Eval. Eng. 12 (4), 264–268.
Wylie, P., Mohanty, K.K., 1999. Effect of wettability on oil recovery by near-miscible gas injection. SPE Reserv. Eval. Eng. 2 (6), 558–564.
Young, L.C., 1990. Use of dispersion relationships to model adverse-mobility-ratio miscible displacements. SPE Reserv. Eng. 5 (3), 309–316.
Zhang, B., 2014. Modeling of bypassed oil recovery in EOS compositional simulation. University of Alberta, Edmonton, Alberta, Master thesis.
Zhou, D., Fayers, F.J., Orr Jr., F.M., 1997. Scaling of multiphase flow in simple heterogeneous porous media. SPE Reserv. Eng. 12 (3), 173–178.